

## AN ABSTRACT OF THE THESIS OF

William C. Krugh for the degree of Master of Science in Geology presented on June 18, 2003.

Title: Fold Growth Due to Kink-band Migration in Repeated Earthquakes, Sierra de Villicum, San Juan, Argentina.

Abstract approved:

---

Andrew J. Meigs

Growth strata geometries and deformed geomorphic surfaces reflect the short-timescale growth of Sierra de Villicum (San Juan Province, Argentina). Accumulated deformation in repeated earthquakes is recorded by the structural geometry of deformed geomorphic surfaces. Through geologic mapping and topographic surveying, six strath terraces were identified on the eastern flank of Sierra de Villicum. A comparison between the modern channel and long terrace profiles indicates that recent deformation is restricted to the eastern half of the study area. In this region, the terrace surfaces are folded  $\sim 15^\circ$  from their original orientation with the fold axes of younger terraces located progressively to the east. This folding has created stepped topography that is interpreted to reflect eastward migration of an active axial surface through repeated earthquakes. Ages for the terrace surfaces were obtained through physical correlation with similar surfaces to the south of the study area. These surfaces are dated at 18700, 6800, and 1500 yr BP using cosmogenic radionuclide exposure age dating (Siame et al., 2002). Deformation rates were calculated by measuring the displacement between the preserved growth axial surface and the active axial surface for each terrace level. On the basis of the inferred terrace ages, the

measured axial surface positions yields average vertical displacement rates of  $1.25 \pm 0.3$  mm/yr and average horizontal displacement rates of  $4.6 \pm 1.0$  mm/yr. The close correlation between historically documented deformation and measured fold displacements suggests the discovery of new evidence for fold growth during a devastating Ms. 7.4 earthquake in 1944.

©Copyright by William C. Krugh  
June 18, 2003  
All Rights Reserved

Fold Growth Due to Kink-band Migration in Repeated Earthquakes,  
Sierra de Villicum, San Juan, Argentina.

by  
William C. Krugh

A THESIS

submitted to

Oregon State University

in partial fulfillment of  
the requirements for the  
degree of

Master of Science

Presented June 18, 2003  
Commencement June 2004

Master of Science thesis of William C. Krugh presented on June 18, 2003.

APPROVED:

---

Major Professor, representing Geology

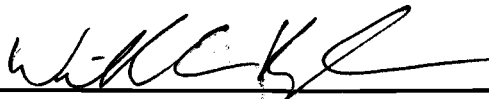
---

Head of the Department of Geosciences

---

Dean of the Graduate School

I understand that my thesis will become part of the permanent collection of Oregon State University libraries. My signature below authorizes release of my thesis to any reader upon request.

A handwritten signature in black ink, appearing to read 'W. C. Krugh', is written over a horizontal line.

William C. Krugh, Author

## ACKNOWLEDGEMENTS

I would like to acknowledge my major advisor Andrew Meigs for his guidance, instruction, and good humor while working with me on this thesis and other projects at OSU. I thank Victor Ramos and Carlos Costa for discussions and field excursions in Argentina. I especially thank Enrique Triep for his help and friendship while staying in San Juan. I would like to acknowledge all of my colleagues at OSU for providing an enjoyable time in Corvallis. I especially thank Sam VanLaningham and Jim Essman for motivation during the winter months. I would also like to thank my parents William and Nancy Krugh and my sister Amanda Krugh for their loving support.

## TABLE OF CONTENTS

	<u>Page</u>
Introduction.....	1
Regional Geologic Setting.....	1
Methodology.....	6
Results.....	10
Geomorphic Surfaces.....	10
Terrace Deformation.....	12
Model.....	18
Discussion.....	25
Conclusion.....	30
Bibliography.....	31
Appendices.....	33
A. Appendix A.....	34
B. Appendix B.....	47

## LIST OF FIGURES

<u>Figure</u>	<u>Page</u>
1. Diagram showing kink-band migration and limb rotation models of fold growth with their respective growth strata geometries.....	2
2. Regional geologic map of San Juan, Argentina.....	3
3. Lithospheric-scale cross-section of the convergent margin of South America ~ 31° S latitude.....	4
4. Geologic map of the southern tip of Sierra de Villicum.....	7
5. Map of terrace surfaces T1-T3 on the eastern flank of Sierra de Villicum, San Juan, Argentina.....	8
6. Map showing the location of profile lines surveyed east of the La Laja fault scarp.....	9
7. Figure showing features of a strath terrace.....	11
8. Figure showing terrace and modern channel longitudinal profiles on the backlimb of Sierra de Villicum.....	13
9. Picture looking S at the La Laja fault scarp.....	14
10a. Sketch showing relationships between topography, folded terraces, and bedrock structure.....	15
10b. View looking south at inclined terrace gravels east of the La Laja fault scarp.....	15
10c. View looking south at folded terrace gravels exposed along a stream channel east of the La Laja fault scarp (see figure 6a for location).....	15
11. Short survey profiles showing stepped topography east of the La Laja fault.....	17
12. Diagram showing proposed style of kink-band migration.....	19
13. Model of fold growth through kink-band migration.....	21



## LIST OF FIGURES (Continued)

<u>Figure</u>	<u>Page</u>
14. Model of fold growth through kink-band migration: Sierra de Villicum, Argentina.....	24
15. Vertical displacement rate (mm/yr).....	28
16. Horizontal displacement rate (mm/yr).....	28

## LIST OF TABLES

<u>Table</u>	<u>Page</u>
1. Table of measured growth axial surfaces and calculated terrace offsets....	23
2. Expected fault slip related to fold growth.....	26

## LIST OF APPENDIX FIGURES

<u>Figure</u>	<u>Page</u>
A1. Map showing cross-section locations across southern end of Sierra de Villicum.....	37
A2. Cross-sections across the southern end of Sierra de Villicum.....	38
A3. Enlarged Crustal-scale model of fold growth for Sierra de Villicum, San Juan Argentina.....	41
A4. Crustal-scale model of fold growth for Sierra de Villicum, San Juan Argentina.....	42
B1. Map showing the location of survey profiles.....	47
B2. AS02 Topographic Profiles.....	48
B3. AS03 Topographic Profiles.....	49
B4. AS04 Topographic Profiles.....	50
B5. AS05 Topographic Profiles.....	52
B6. AS06 Topographic Profiles.....	53
B7. AS08 Topographic Profiles.....	54

# **Fold Growth Due to Kink-band Migration in Repeated Earthquakes, Sierra de Villicum, San Juan, Argentina.**

## **Introduction**

Growth strata and deformed geomorphic features record the kinematic evolution of fault-related folds. Through their depositional and structural geometries, these markers provide critical information for evaluating models of fold growth, establishing displacement rates on blind thrusts, and developing a reliable estimation of seismic hazard (Figure 1) (Lavè and Avouac, 2000; Suppe, 1992; Verges et al., 1996). Whereas these records are often used to identify active structures (Dolan et al., 2003; Mueller and Suppe, 1997; Shaw et al., 2002; Suppe et al., 1997; Suppe, 1992), existing studies do not clearly resolve mechanisms of fold growth at the scale of discrete earthquake events. This paper focuses on the geomorphic and geologic evidence for the growth of Sierra de Villicum, Argentina as the result of kink-band migration in repeated earthquakes, including an earthquake of Ms 7.4 in 1944.

## **Regional Geologic Setting**

Sierra de Villicum is a historically active, mountain-range-scale fault-related fold located in the Eastern Precordillera of San Juan, Argentina (Figures 2 & 3). Situated between the thin-skinned Precordillera fold-and-thrust belt to the west and the basement-involved Sierras Pampeanas thrust belt to the east, the Eastern Precordillera exhibits characteristics of both structural provinces (Fielding and Jordan, 1988; Jordan et al., 1983; Ramos et al., 2002). Sierra de Villicum is a west-vergent thrust sheet involving an Upper Cambrian through Middle Miocene

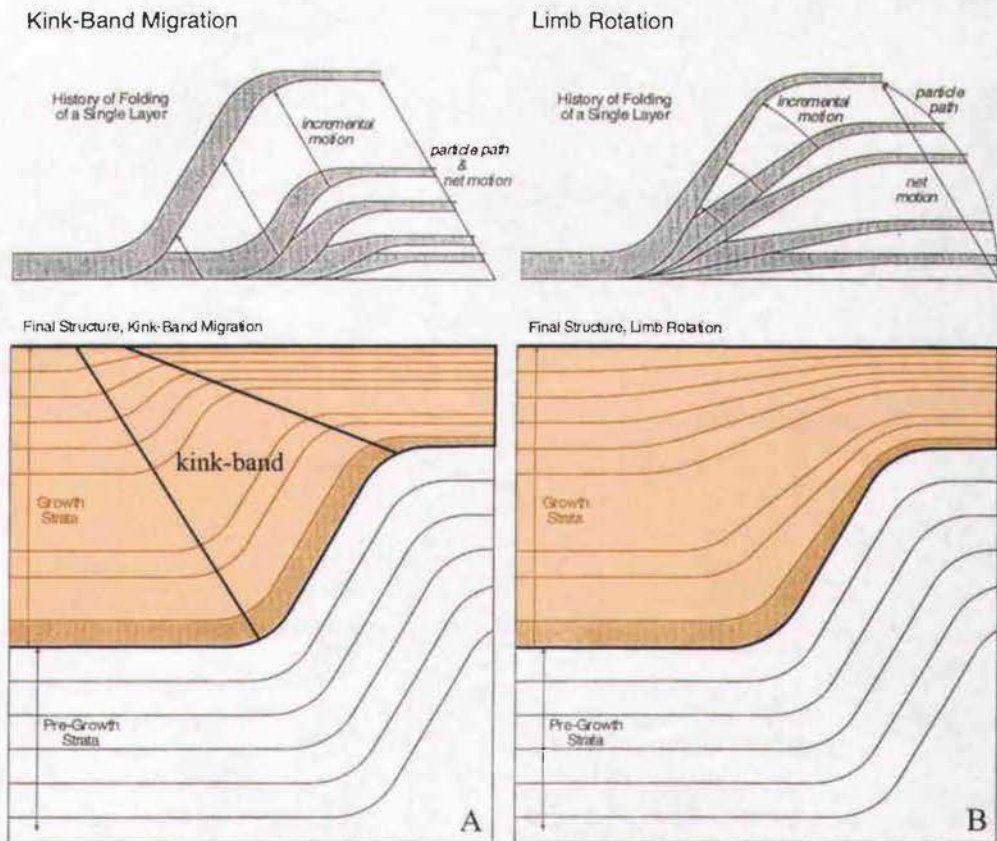


Figure 1 Diagram showing kink-band migration and limb rotation models of fold growth with their respective growth strata geometries. Both models share similar geometries of pre-growth strata (shown in white), but have different growth strata (shown in orange) geometries that reflect the different styles of fold growth. A) Models of fold growth through kink-band migration have narrowing upward kink-bands and parallel bedding within their growth strata. B) In contrast, limb rotation models of fold growth have progressively shallower dips within younger growth strata. Modified from Suppe et. al., 1997.

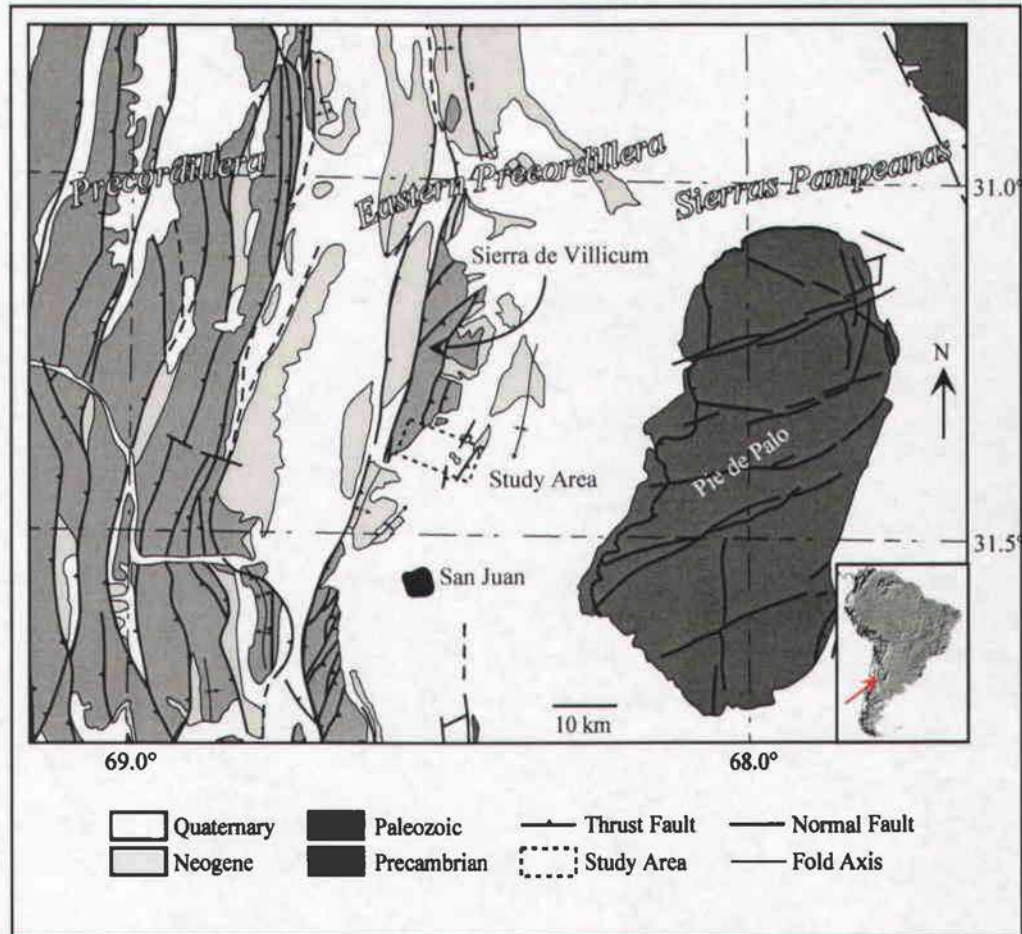


Figure 2 Regional geologic map of San Juan, Argentina. Sierra de Villicum is located at the center of the map with the Precordillera thin-skinned fold and thrust belt to the west and the Sierras Pampeanas basement-involved uplifts to the east. Modified from Ragona et al. (1995).

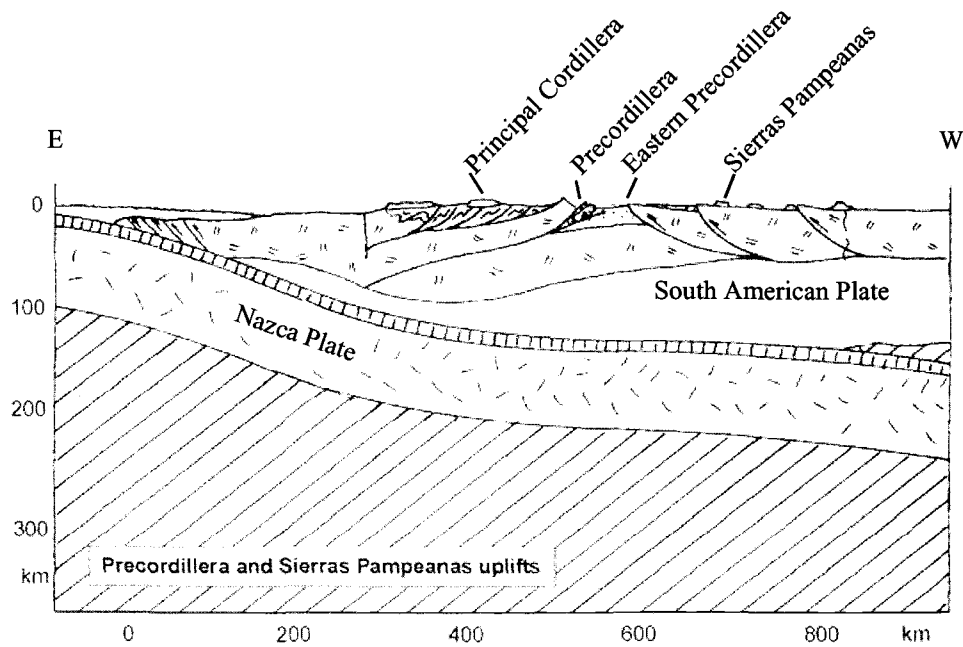


Figure 3 Lithospheric-scale cross-section of the convergent margin of South America  $\sim 31^\circ$  S latitude. Notice the shallow subduction angle of the Nazca plate. Structural provinces within the overriding South American plate are highlighted. Modified from Ramos et al. (2002).

stratigraphic sequence similar to the ~ 4 km thick thrust sheets of the Precordillera (von Gosen, 1992). In contrast, microseismicity beneath the range is focused along a west-dipping plane oriented  $35^{\circ}/315^{\circ}$  (dip/dip-direction) and extends from 5 to 35 km depth (Smalley et al., 1993). These seismic data suggest that an active, east-vergent, basement-involved fault exists beneath the thin-skinned thrust sheet. On January 15<sup>th</sup>, 1944 San Juan, Argentina experienced a devastating Ms 7.4 earthquake. Surface deformation associated with the earthquake was observed on the eastern flank of Sierra de Villicum (Bastias et al., 1985; Groeber, 1944; Harrington, 1944; Paredes and Uliarte, 1988). Surface rupture with ~ 60 cm of coseismic displacement was documented along the ~ 6 km long La Laja fault (Harrington, 1944). Together, the 1944 earthquake, the microseismicity, and the structural geometry of Sierra de Villicum suggest a link between the locus of surface deformation and an active, east-vergent, basement-involved structure at depth.

A suite of deformed strath terraces record the progressive growth of Sierra de Villicum and allow for description, measurement, and characterization of fold growth associated with repeated earthquakes (Suppe et al., 1997; Suppe, 1992). These markers place constraints on the rate of folding, the geomorphic signal of fold growth, and the development of growth strata during individual earthquakes. Thus, these preserved geomorphic markers make Sierra de Villicum a favorable locale for linking short and intermediate timescale fold growth.



## Methodology

Mapping on the backlimb of Sierra de Villicum constrains the near-surface bedrock geology, the structural geometry of the fold, and the distribution and relative ages of terraces (Figures 4 & 5). A ~54 km<sup>2</sup> study area was mapped at a scale of 1:30,000 on an aerial photograph base. Bedrock descriptions and structural data were obtained from outcrops exposed along stream channels. Individual terraces were differentiated by their physical characteristics, relative positions, and elevation above the modern channel. Terrace mapping ~15 km to the southwest allows for correlation with a suite of surfaces dated on the basis of cosmogenic radionuclide (CRN) exposure ages (Siame et al., 2002).

The structural and kinematic style of Sierra de Villicum was quantified through combined field mapping and detailed topographic surveying. Selected terrace surfaces and modern channels were surveyed across the full width of the backlimb of Sierra de Villicum. Localized terrace surveys focused on an area east of the La Laja fault where stepped topography is apparently coincident with the locus of active surface deformation (Figure 6). Terrace surface elevations were collected by laser-theodolite surveys from a series of GPS located survey stations. Multiple survey stations were required because of vegetation obstructions and range limitations of the laser-theodolite. To minimize the vertical and horizontal error of individual GPS locations, overlapping data points were surveyed from neighboring stations. By co-registering these data points, adjacent survey stations were tied together to create a continuous set of topographic data.



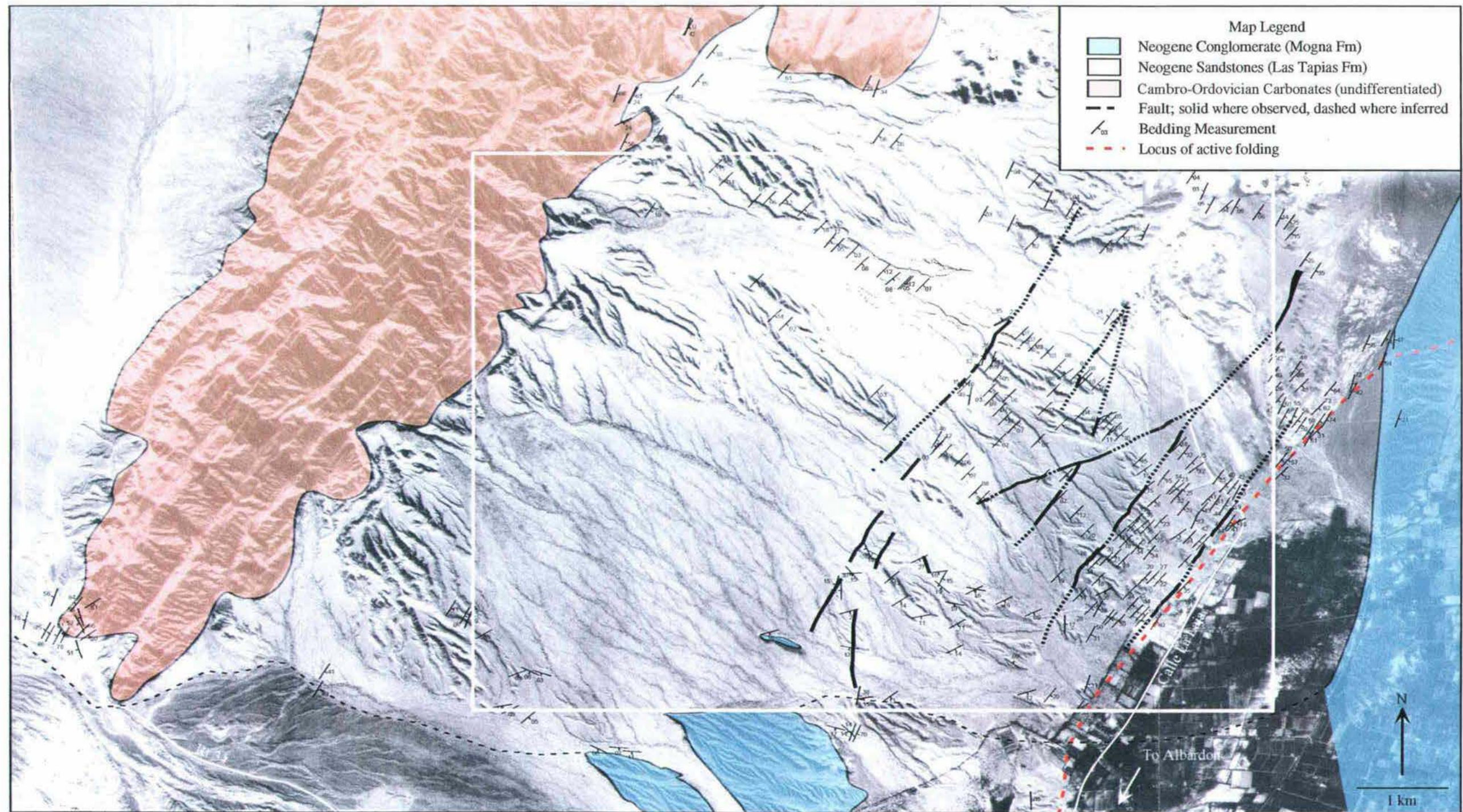


Figure 4 Geologic map of the southern tip of Sierra de Villicum. The location of Figure 5 is outlined in white.



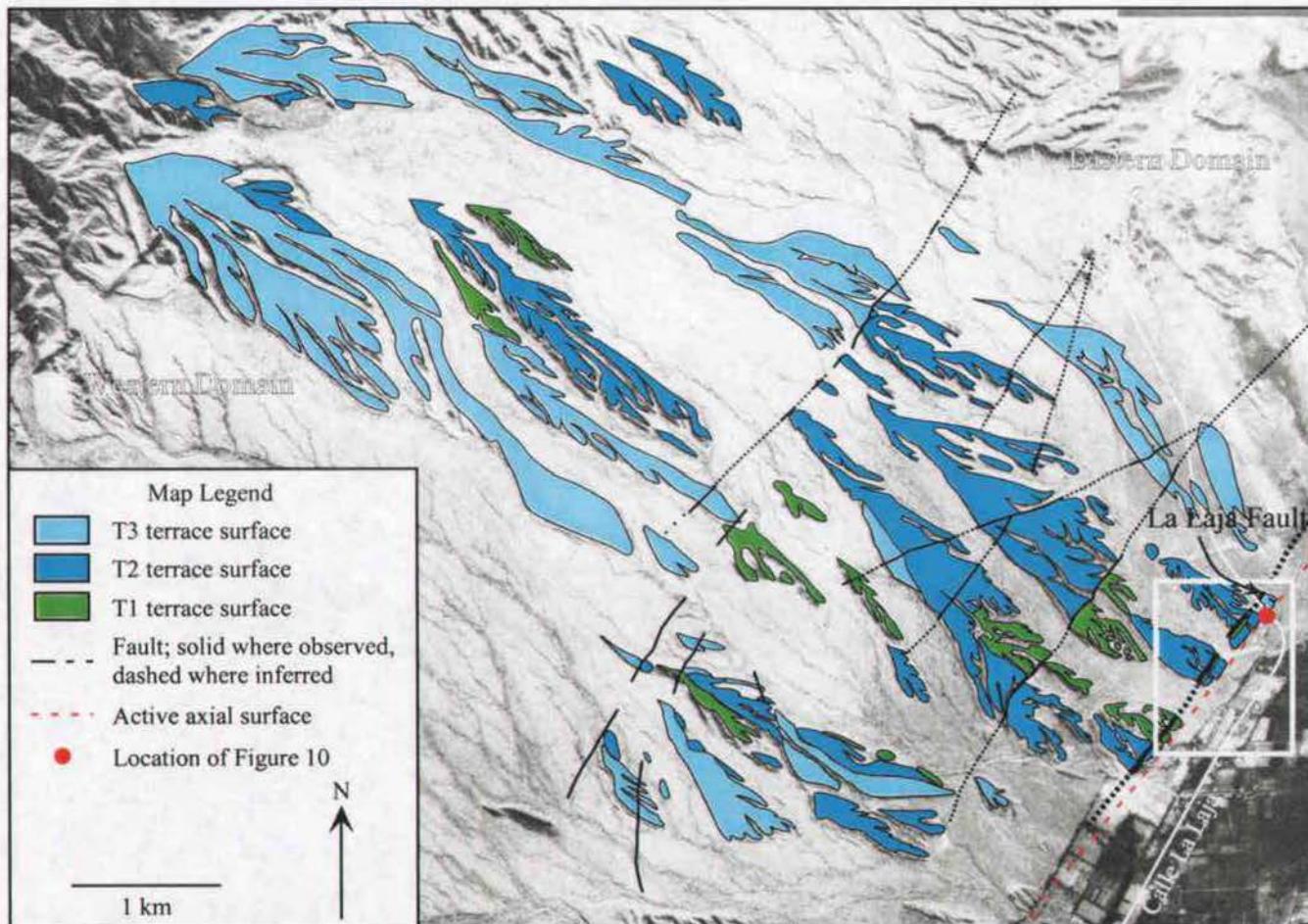


Figure 5 Map of terrace surfaces T1-T3 on the eastern flank of Sierra de Villicum, San Juan, Argentina. The location of Figure 6 is outlined by a white box. The location of Figure 10 is marked by a red dot.



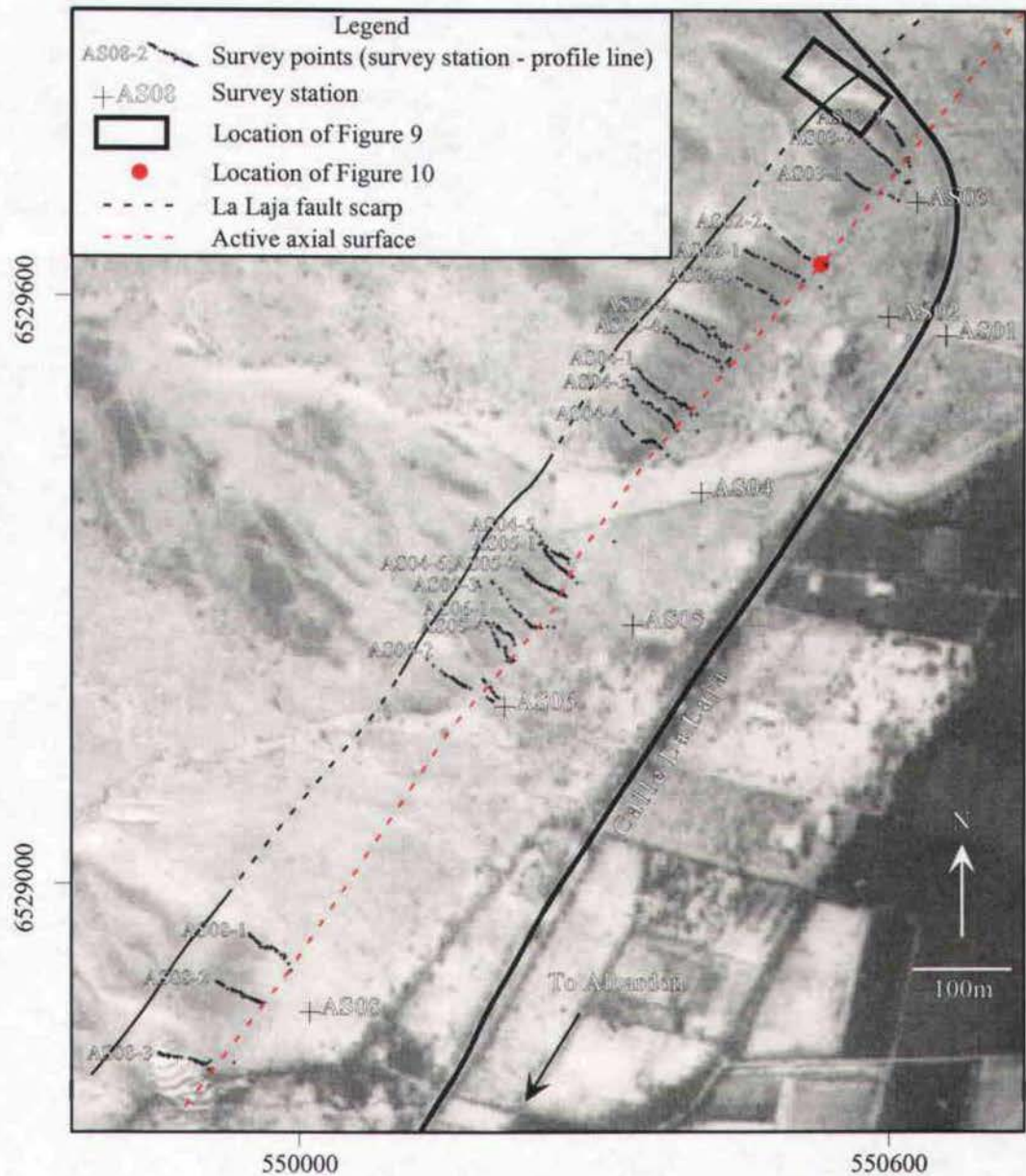


Figure 6 Map showing the location of profile lines surveyed east of the La Laja fault scarp. Individual terrace profiles are located in Survey Appendix. The location of Figure 10 is marked by a red dot.

The geologic mapping and topographic survey results form the basis of a model of the progressive growth of Sierra de Villicum. This model reconciles bedrock and terrace structural geometries and fold-related topography. Deformation rates were calculated on the basis of correlation with the terrace ages of Siame (2002).

## **Results**

### **Geomorphic Surfaces**

Six terraces were identified on the eastern flank of Sierra de Villicum. Each terrace consists of a low-relief bedrock erosional surface (strath) that is overlain by 1-3 meters of poorly-sorted limestone-and-dolomite-clast gravels (Figure 7). The relative ages of the terraces were determined by their distribution, elevation above the modern channel, and differences in surface morphology and composition. Sequentially younger terraces are inset into older terraces and occupy successively lower elevations above the modern channel. Older terraces are more dissected, have lower surface relief, and have a higher concentration of varnished chert clasts. Based on these observations, the terraces were classified T1 = oldest to T6 = youngest. Terraces T1-T3 extend along the entire width of the backlimb of Sierra de Villicum whereas terraces T4-T6 are restricted to areas adjacent to locally active structures (Figure 5).

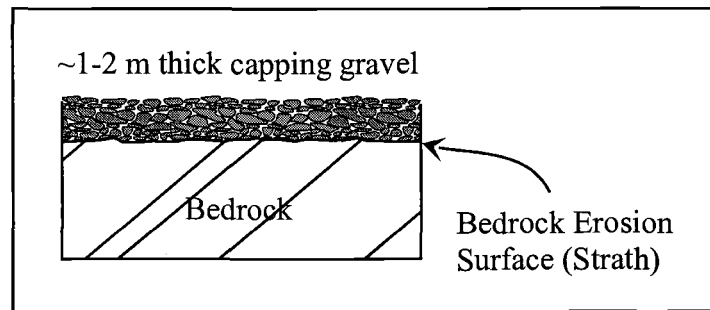


Figure 7  
Figure showing features of a strath terrace.

The surface morphology and longitudinal profiles of these strath terraces are relatively planar, similar to those of the modern channel (Figure 8). Active channels on Sierra de Villicum are ephemeral, mixed bedrock and alluvial channels inset within a very poorly sorted, thin ( $\sim 1\text{-}2\text{ m}$ ) gravel veneer. The overall gradient for both the modern channel and terrace surfaces is  $\sim 3^\circ\text{E}$ .

### **Terrace Deformation**

Terrace deformation on the backlimb of Sierra de Villicum is partitioned into eastern and western domains (Figures 5 and 8). In the western domain, bedrock structure is characterized by broad open folds. Terrace surfaces are inclined  $\sim 3^\circ$  to the east and are neither folded nor faulted. In the eastern domain, several faults offset terrace surfaces. Several of these faults, including the La Laja fault, are reverse faults that have the same dip as parallel bedding planes. The La Laja fault scarp is identified in airphotos as a topographic lineament and in outcrop by truncated terrace straths where Neogene bedrock overlies terrace gravels (Figure 9). Neogene bedrock strata are not duplicated by the fault and fault dip is the same as adjacent bedding dips in both the hanging wall and footwall.

Each of the strath terraces is folded in a narrow region to the east of the La Laja fault (Figure 6). The structural style and geometric relationships of the folded terraces are well represented in southeast-draining stream channels transverse to the northeast trending structure (Figure 10). T2, for example, forms an east-facing monocline as indicated by a change in dip from  $\sim 3^\circ\text{E}$  to  $\sim 18^\circ\text{E}$  from west to east,

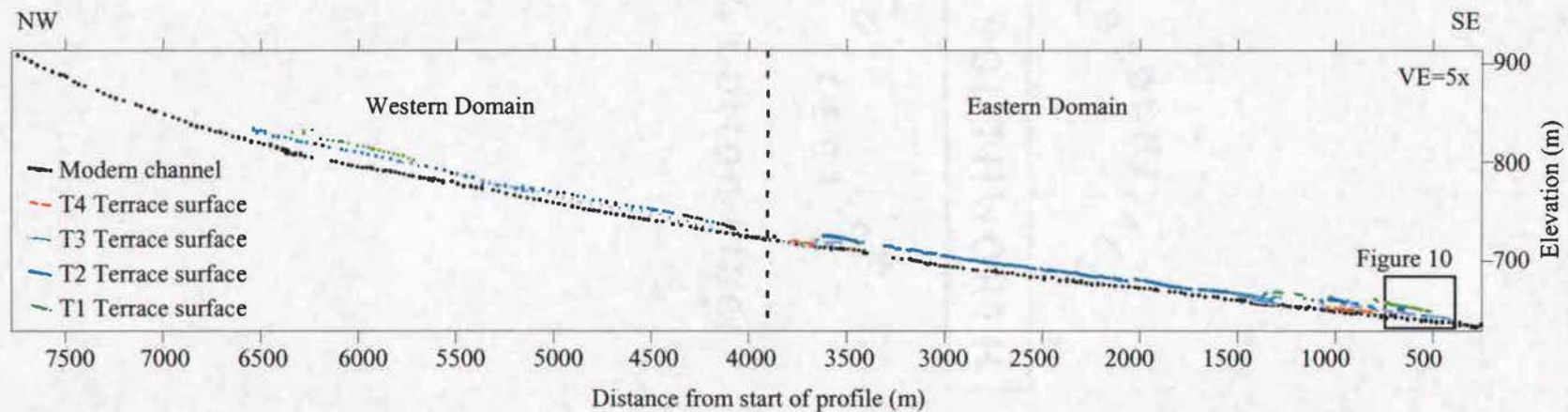
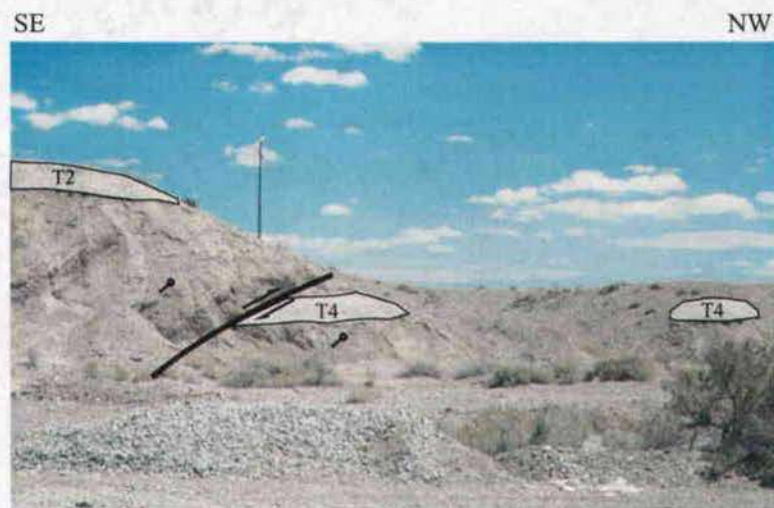


Figure 8 Figure showing terrace surface and modern channel longitudinal profiles on the backlimb of Sierra de Villicum. Notice the concave upward shape and parallel nature of the surfaces. The dashed line marks the boundary between the Eastern Domain (terraces folded and cut by faults) and the Western Domain (terraces not folded or faulted). The locus of active folding and position of Figure 10 are shown by the box.





**Figure 9** Picture looking S at the La Laja fault scarp. Las Tapias Formation sandstone in the hangingwall of the fault structurally overlies T4 terrace gravels

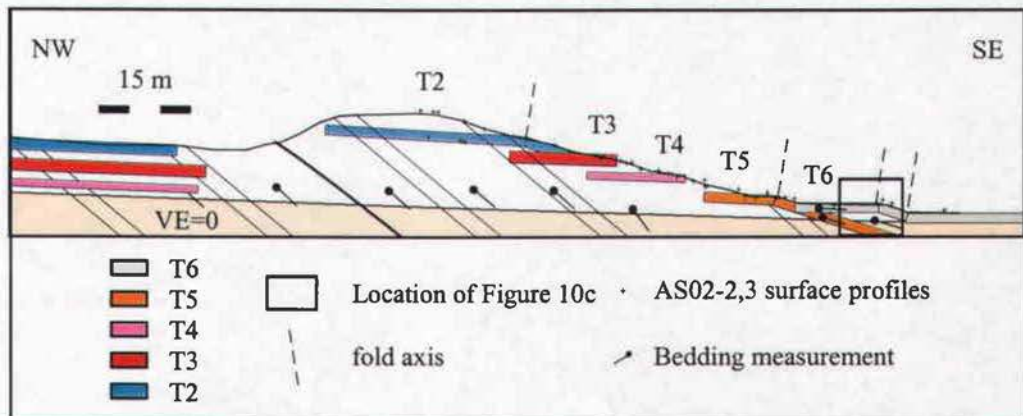


Figure 10a Sketch showing relationships between topography, folded terraces, and bedrock structure.

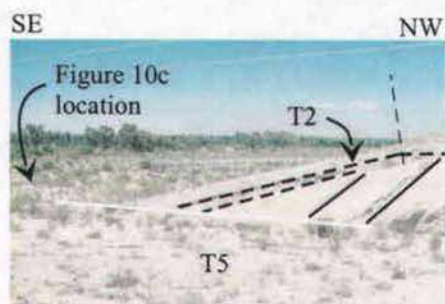


Figure 10b View looking south at inclined terrace gravels east of the La Laja fault scarp. Heavy dashed lines represent position of strath surfaces. Thin dashed line represents approximate location of T2 growth axial surface. The white line represents the top of the inset T5 terrace surface.

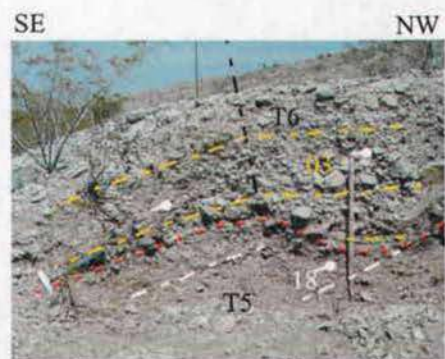


Figure 10c View looking south at folded terrace gravels exposed along a stream channel east of the La Laja fault scarp (see figure 6a for location). Inclined T5 deposits are truncated (dashed red line) and unconformably overlain by ~ horizontal T6 gravels (dashed yellow line). To the east of the dashed black line (fold axis) the contact between the two deposits is conformable. Rock hammer and 70 cm "broom" for scale.



respectively. In contrast, the Neogene bedrock underlying T2 has a uniform dip of  $\sim 40^\circ\text{E}$  on both sides of the fold axis in the T2 terrace. T5 is inset and crosses the inclined T2 terrace at this locality. Ten meters east of the T2 monocline, the T5 terrace is folded and unconformably overlain by a younger, sub-horizontal gravel deposit (T6), which itself is folded to the east of the T5 fold axis. Figure 10c shows the difference in depositional contacts on either side of the T6 fold axis. West of the T6 axis, T5 gravels dip  $18^\circ\text{E}$  whereas the T6 terrace gravels dip  $3^\circ\text{E}$  and the contact is an unconformity. To the east, both the T5 and T6 gravels dip  $18^\circ\text{E}$  and have a conformable contact. The folded T6 gravels are unconformably overlain by a horizontal gravel deposit that has a surface elevation  $\sim 50$  cm above the modern channel. This outcrop demonstrates that individual terraces are marked by discrete fold axes that are located progressively eastward within younger terraces.

A series of east-facing hillslopes, east of the La Laja fault scarp, are characterized by step-like morphology (Figure 11). These topographic features consist of  $\sim$  flat tread surfaces separated by inclined slopes. Tread surfaces decrease in elevation from west to east. Several of these treads correspond with the elevations of mapped terrace surfaces. In outcrop, the intersection between tread surfaces and inclined slopes appears to correspond with the position of fold axes within the respective terrace gravels.

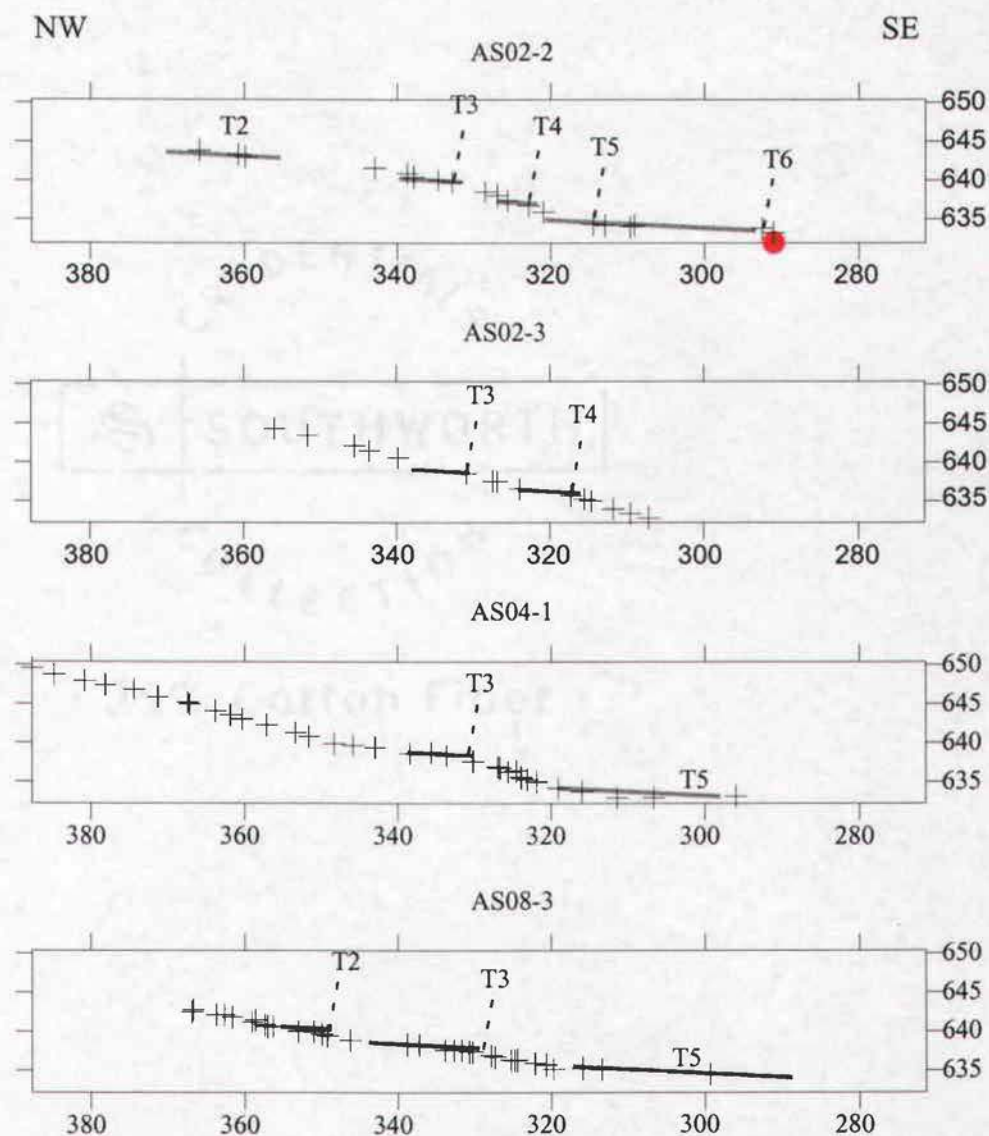


Figure 11 Short survey profiles showing stepped topography east of the La Laja fault. Interpreted terrace surfaces (treads) are shown in grey. The location of a folded T6 gravels (Figure 10b) is marked by the red dot. All of the short survey profiles are available in the Survey Appendix. Growth axial surfaces are marked by short dashed lines. No vertical exaggeration.

## Model

The observed geometric relationships between bedrock structure, folded terraces, and topography place constraints on the structural style and kinematic history of Sierra de Villicum. Any viable model of fold growth must reconcile these features. A model of fold growth via kink-band migration best explains the topography, folded terrace geometries, and bedrock orientations observed east of the La Laja Fault.

Kink-band migration involves folding caused by motion of an axial surface(s) relative to bedrock (Figure 12). The region between two corresponding axial surfaces is termed a "kink-band". In growing structures, one or both of these axial surfaces is free to move relative to bedrock. This type of fold axis is called an active axial surface whereas a fold axis that is stationary with respect to the bedrock is called a fixed axial surface. As an active axial surface migrates, rock is instantaneously rotated about the axis and translated onto the fold limb (Suppe, 1983). Continued migration of axial surfaces, relative to one another, translates additional material onto the fold limb and results in lengthening of the fold limb. Folds that grow by kink-band migration are characterized by narrowly-defined hinges and fold limbs with parallel bedding and constant dip. Both of these characteristics describe the bedrock structure and folded terrace geometries of Sierra de Villicum.

Strata formed coevally with fold growth are referred to as growth strata. Through their structural and depositional geometries, growth strata act as markers

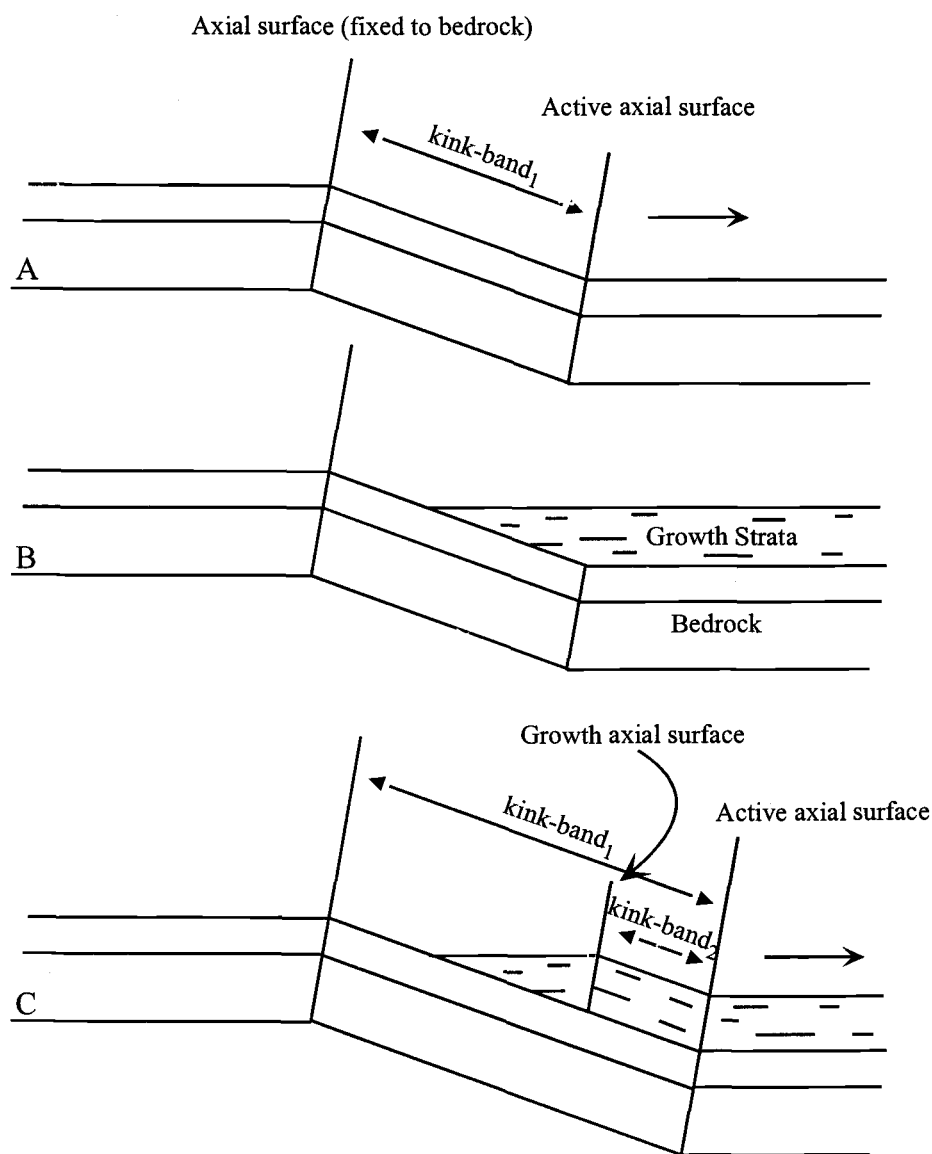


Figure 12 Diagram showing proposed style of kink-band migration. A) The axial surface on the left is fixed with respect to bedrock while the active axial surface (on the right) is free to move relative to the bedrock. The  $kink-band_1$  is the area of folded bedrock between the two axial surfaces and reflects the net motion of the active axial surface. B) Strata deposited coeval with fold growth are called growth strata. C) Continued fold growth increases the width of  $kink-band_1$  (within bedrock).  $kink-band_2$  (within the growth strata) is narrower than  $kink-band_1$  and reflects the growth of the fold following deposition of the growth strata.  $kink-band_2$  is bound on the left by a growth axial surface.

that constrain the timing and style of structural growth (Suppe et al., 1997; Suppe, 1992). For a model of fold growth due to kink-band migration, growth strata record the position and movement of active axial surfaces in relation to their corresponding fixed axial surfaces. In growth strata, a fixed axial surface records the initial position of an active axial surface prior to folding of the strata (Figure 13). These fixed axial surfaces separate folded and unfolded growth strata and are therefore called growth axial surfaces.

As an axial surface migrates, growth strata are rotated and incorporated into the fold limb along with older strata. Because older growth strata have endured more folding, kink-bands become progressively narrower within younger growth strata (Figure 1) (Suppe, 1992). The horizontal distance between two or more growth axial surfaces of known age is a function of the migration rate of the active axial surface relative to the growth axial surface. As a result, the growth axial surface is located closer to the active axial surface in successively younger growth strata (Figure 12). Whereas the active axial surface is common to all growth strata, the position of a growth axial surface varies among different strata (Figure 13). Therefore, the horizontal and vertical components of fold growth can be measured from the differential elevation and horizontal offset between active axial surfaces and growth axial surfaces along individual terraces.

Based on this model of kink-band migration, fold growth should be reflected by the topography of the folded terrace surfaces. Assuming each terrace surface forms with the same gradient as the modern channel (Figure 8), terraces



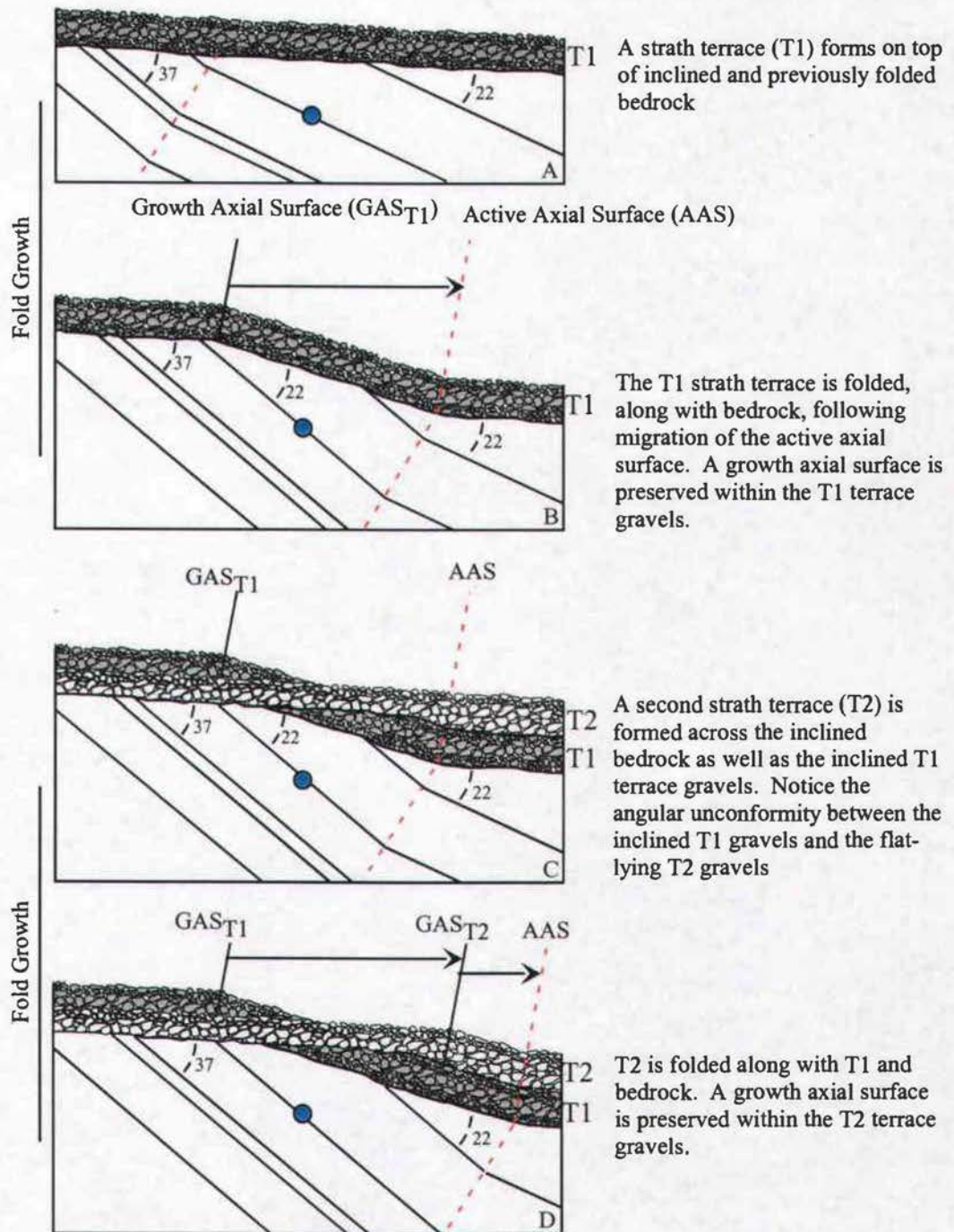


Figure 13 Model of fold growth through kink-band migration. Figures A-D show a sequence of folding that illustrates the connection between bedrock structure, terrace depositional and structural geometries, and topography. The blue dot reflects the position of an individual particle during fold growth.



become inclined only after folding (Figure 13). An inflection between shallowly inclined and moderately inclined terrace surfaces thus represents a preserved growth axial surface as well as the location of the active axial surface prior to folding and uplift of the terrace. These growth strata relationships are observed in the folded terraces on the eastern flank of Sierra de Villicum. The growth axial surfaces of younger terraces are located progressively to the east, effectively recording eastward migration of the active axial surface.

The positions of preserved growth axial surfaces were located on the topographic profiles for each of the mapped terrace surfaces by identifying this inflection (Figures 6 & 11). All measurements were made in relation to the position of the interpreted active axial surface. The average positions of growth axial surfaces are presented in Table 1. Because of the overlapping relationship of terrace deposits, these measurements do not represent the true offset between the growth axial surface and active axial surface of an individual terrace, but rather the difference between the growth axial surface and the intersection of the active axial surface with the modern channel (Figure 14). The following formulas were used to calculate the true horizontal and vertical offset of the growth axial surface from the active axial surface along individual terraces (see Figure 14 for variable definitions).

$$X_t = ((X + Z \cdot \tan(f)) \cdot \sin(a) / \sin(b) \cdot \cos(c))$$

$$Z_t = ((X + Z \cdot \tan(f)) \cdot \sin(a) / \sin(b) \cdot \sin(d) / \sin(e))$$

Table 1. Table of measured growth axial surfaces and calculated terrace offsets

	elevation above SL (m)	Z = elevation above modern surface (m)	distance from survey station (m)	X = distance from active axial surface (m)		Zt = vertical terrace offset (m)	Xt = horizontal terrace offset (m)
T1	649.3	15.1	376.2	87.4		23.2	85.1
T2	641.3	7.1	340.0	51.2		13.5	49.5
T3	638.6	4.3	325.3	36.6		9.6	35.2
T4	637.2	2.9	317.4	28.6		7.5	27.5
T5	635.1	0.8	311.8	23.1		6.0	21.9
T6	634.8	0.5	291.0	2.2		0.6	2.2
modern	634.3	0.0	288.8	0.0		0.0	0.0

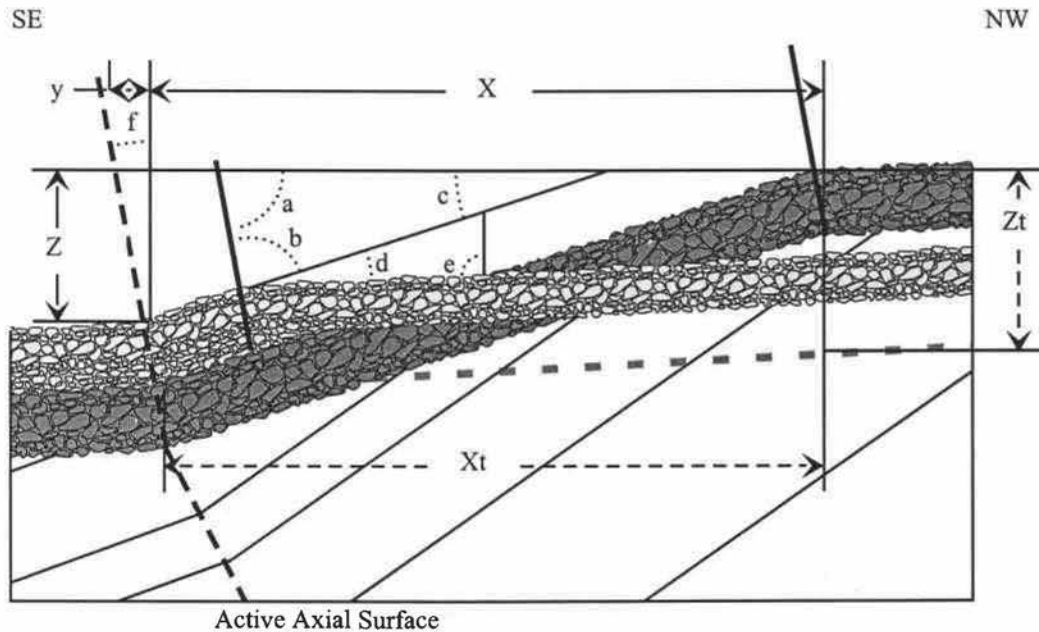


Figure 14 Model of fold growth through kink-band migration: Sierra de Villicum, Argentina. The variables used to calculate the true vertical and horizontal offset of a given terrace surfaces are shown on the figure and defined below.

$a$  = angle between the horizontal and the active axial surface

$b$  = angle between the active axial surface and the inclined terrace tread

$c$  = inclination of the inclined tread surface

$d$  = angle between the ~ flat terrace tread and inclined tread surface

$e$  = angle between the vertical and the ~flat terrace tread

$f$  = angle between the vertical and the active axial surface

$X$  = distance between the growth axial surface for a given terrace and the surface expression of the active axial surface (measured from topographic profiles)

$Z$  = elevation of the terrace surface above the elevation of the modern channel (measured from topographic profiles)

$X_t$  = true horizontal offset for a given terrace surface  
 $= ((X + Z \cdot \tan(f)) \cdot \sin(a) / \sin(b) \cdot \cos(c))$

$Z_t$  = true vertical offset for a given terrace surface  
 $= ((X + Z \cdot \tan(f)) \cdot \sin(a) / \sin(b) \cdot \sin(d) / \sin(e))$

The true horizontal and vertical offsets for the mapped terrace surfaces are presented in Table 1.

### **Discussion**

The La Laja fault is interpreted as a flexural slip fault associated with fold growth on the eastern flank of Sierra de Villicum. This interpretation is supported by the bedding parallel orientation of the fault. Additionally, the La Laja fault was not observed to truncated bedding anywhere along its ~ 6km trace. Assuming that the La Laja fault is a secondary flexural slip fault, then fault slip should be tied to fold growth. Using the horizontal offset between the active axial surface and growth axial surfaces as a measure of fold growth, the corresponding slip on the La Laja fault can be calculated. Bedding parallel slip during kink style folding is related to the thickness of the fold limb above the fault plane (Suppe, 1983). Because the Las Tapias sandstone is inclined ~40°E on both sides of the La Laja fault, limb thickness above the fault increases to the east. The bedrock limb thickness underlying each growth axial surface was obtained from Figure 10a by measuring perpendicular to the projected La Laja fault trace. Using the equation;  $\text{fault slip} = 2 \times \text{limb thickness} \times \tan(\text{change in dip}/2)$ , the expected fault slip for a given limb thickness was calculated (Table 2). Because the limb thickness increases to the east, the maximum thickness of the fold occurs at the active axial surface. Additionally, because fault slip increases with limb thickness, the

Table 2. Expected fault slip related to fold growth

	Limb thickness (m)	Calculated Dip Slip (m)
T1	18.4	4.9
T2	23.8	6.3
T3	30.9	8.1
T4	35.0	9.2
T5	39.7	10.5
T6	45.6	12.0
AAS	47.8	12.6

Differential slip (m)			
	dip slip	z	x
T1-T2	1.4	0.9	1.1
T2-T3	1.9	1.2	1.5
T3-T4	1.1	0.7	0.8
T4-T5	1.2	0.8	0.9
T5-T6	1.6	1.0	1.2
T6-AAS	0.6	0.4	0.4

Net slip (m)			
	dip slip	z	x
T1	7.7	5.0	5.9
T2	6.3	4.1	4.9
T3	4.4	2.9	3.4
T4	3.4	2.2	2.6
T5	2.1	1.4	1.6
T6	0.6	0.4	0.4

maximum slip on the fault can be calculated from the limb thickness measured at the active axial surface. Based on the model of fold growth through kink-band migration, the fault slip calculated for each growth axial surface represents the net displacement on the fault. By subtracting the net displacements obtained from older growth axial surfaces, the incremental slip on the fault can be calculated (Table 2). The calculated vertical and horizontal displacements are on the same order of magnitude as those observed on the truncated terrace surfaces.

Controls on the absolute age of the terraces at La Laja are not available. An estimate of the horizontal and vertical displacement rates can be obtained by using the absolute ages obtained on similar terrace surfaces ~ 15km southwest of the study area, herein referred to as the “southern sequence”. Terraces in the two areas were physically correlated through geologic mapping. Siame et al., (2002) obtained cosmogenic radionuclide (CRN) exposure ages of 18700, 6800, and 1500 yr BP for terrace surfaces elevated  $11 \pm 1$  m,  $6 \pm 2$  m, and  $\sim 0.6$  m above the modern channel, respectively. In the study area, the 18700 yr BP age surface could correlate with either the T1 or T2 terrace. The reason for this uncertainty is that the cosmogenic samples were taken on a different part of the structure and neither T1 nor T2 could be directly tied to the southern terrace sequence. Because of this uncertainty, a range of displacement rates was calculated from the CRN data (Figures 15 & 16). The 18700 yr BP age suggests a vertical displacement rate of  $1.0 \pm 0.3$  mm/yr and a horizontal displacement rate of  $3.6 \pm 1.0$  mm/yr. Similarly, the 6800 yr BP age surface could correlate with either the T2, T3 or T4 terraces,

Figure 15 Vertical displacement rate (mm/yr)

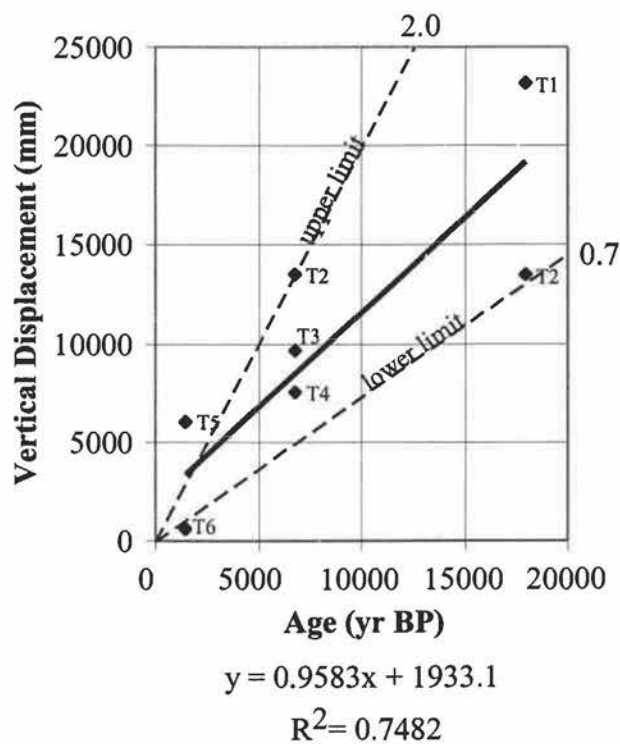
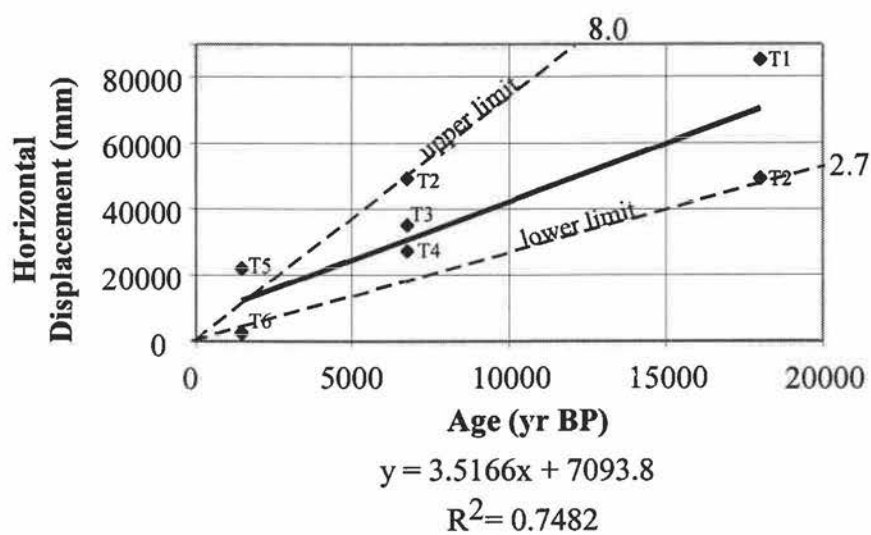


Figure 16 Horizontal displacement rate (mm/yr)



resulting in a vertical displacement rate of  $1.5 \pm 0.3$  mm/yr and a horizontal displacement rate of  $5.5 \pm 1.2$  mm/yr. Because the  $\sim 0.6$  m elevation is within the variability of relief observed on the modern channel, the 1500 yr BP age likely corresponds to either the T5 or T6 terrace surfaces, yielding an uplift rate of  $2.2 \pm 1.8$  mm/yr and a shortening rate of  $8.0 \pm 6.6$  mm/yr.

Because samples used for cosmogenic radionuclide exposure dating begin producing nuclides only when exposed to cosmic radiation, the ages obtained for the terrace surfaces include CRNs accumulated during erosional exhumation, transportation, and in situ production on the terrace surface (Anderson et al., 1996). Assuming that the lowest dated terrace ( $\sim 0.6$  m above the active channel) is associated with the modern channel, the 1500 yr BP age may represent the inheritance of samples during exhumation and transport. If correct, terrace ages may be systematically younger by 1500 yrs. This hypothesis could explain the large errors associated with the range of uplift and shortening rates obtained from the 1500 yr BP age for the T5 and T6 terraces. The calculated deformation rates incorporate error in correlating specific surfaces in the southern terrace sequence terraces to those in the study area as well as the error associated with measurement of growth axial surface positions from the topographic datasets.

Fold growth and geomorphic processes creating the terraces are offset in time. Assuming that the  $\sim 50$  cm offset of the T6 terrace represents the typical fold growth for Sierra de Villicum during a single earthquake, the meter scale offsets between individual terrace surfaces thus reflects deformation accumulated over



several events. This hypothesis is supported by the identification of growth axial surfaces that correspond with ~ the same terrace surface (T5 and T6 in outcrop shown in Figure 10). This relationship suggests that several fold generating earthquakes occur between the geomorphic processes of terrace formation and abandonment.

Fold growth associated with the 1944 earthquake is interpreted to have produced the folded T6 terrace. Identified only to the east of the La Laja fault, the T6 strath has an elevation ~ 50 cm above the active channel. This relief is similar to the ~30 to 60 cm of vertical offset reported on the La Laja fault during the 1944 earthquake.

### **Conclusion**

Observed deformation of strath terraces on the backlimb of Sierra de Villicum is consistent with a model of fold growth through kink-band migration. Sequential preservation of growth axial surfaces within terrace gravels allows for the quantification of fold growth. The vertical displacement rate is between ~ 2.0 and 0.7 mm/yr whereas the horizontal displacement rate is between ~ 8.0 and 2.7 mm/yr. Furthermore, a set of measured, geometric relationships describe uplift on the same scale (~30-60cm) as reported displacement along the La Laja fault during the 1944 earthquake. Because the La Laja fault is bedding parallel, it occurs within an area of steeply dipping bedrock, and it is associated with the locus of active deformation, it can be classified as a flexural slip fault related to fold growth of Sierra de Villicum.

## Bibliography

- Anderson, R.S., et al., 1996, Explicit treatment of inheritance in dating depositional surfaces using in situ (super 10) Be and (super 26) Al: *Geology* (Boulder), v. 24, p. 47-51.
- Bastias, H.E., et al., 1985, Dos zonas de fallamiento Pliocuaternario en la Precordillera de San Juan Translated: The Plio-Quaternary fault zone in the Precordillera of San Juan: *Actas del Congreso Geológico Argentino*, v. 9, p. 329-341.
- Dolan, J.F., et al., 2003, Recognition of Paleoearthquakes on the Puente Hills Blind Thrust Fault, California: *Science*, v. 300, p. 115-118.
- Fielding, E.J. and Jordan, T.E., 1988, Active deformation at the boundary between the Precordillera and Sierras Pampeanas, Argentina, and comparison with ancient Rocky Mountain deformation: *Memoir - Geological Society of America*, v. 171, p. 143-163.
- Groeber, P., 1944, Movimientos tectonicos contemporaneos y un nuevo tipo de dislocaciones: *Notas del Museo de La Plata*, v. 9, p. 363-375.
- Harrington, H.J., 1944, El sismo de San Juan; del 15 de Enero de 1944: Buenos Aires, Corporacion para la promocion del intercambio, S. A., 79 p.
- Jordan, T.E., et al., 1983, Andean tectonics related to geometry of subducted Nazca Plate: *Geological Society of America Bulletin*, v. 94, p. 341-361.
- Lavè, J. and Avouac, J.P., 2000, Active folding of fluvial terraces across the Siwaliks Hills, Himalayas of central Nepal: *Journal of Geophysical Research, B, Solid Earth and Planets*, v. 105, p. 5735-5770.
- Mueller, K. and Suppe, J., 1997, Growth of Wheeler Ridge anticline, California; geomorphic evidence for fault-bend folding behaviour during earthquakes: Special issue; fault-related folding *Journal of Structural Geology*, v. 19, p. 383-396.
- Paredes, J.D. and Uliarte, E., 1988, Analisis morfotectonico del sistema de fallamiento precordillera oriental, San Juan, Argentina: II Reunion Sudamericana del Proyecto 206 del IGCP, Santiago Chile.
- Ramos, V. and Vujovich, G., 2000, Hoja Geològica San Juan, escala 1:250.000.: Servicio Geològico Minero Argentino, Boletìn, Buenos Aires, v. 245, p. 82.

- Ramos, V.A., et al., 2002, The Pampean flat-slab of the Central Andes: *Journal of South American Earth Sciences*, v. 15, p. 59-78.
- Shaw, J.H., et al., 2002, Puente Hills blind-thrust system, Los Angeles, California: *Bulletin of the Seismological Society of America*, v. 92, p. 2946-2960.
- Siame, L.L., et al., 2002, Seismic hazard reappraisal from combined structural geology, geomorphology and cosmic ray exposure dating analyses; the eastern Precordillera thrust system (NW Argentina): *Geophysical Journal International*, v. 150, p. 241-260.
- Smalley, R., Jr., et al., 1993, Basement seismicity beneath the Andean Precordillera thin-skinned thrust belt and implications for crustal and lithospheric behavior: *Tectonics*, v. 12, p. 63-76.
- Suppe, J., 1983, Geometry and kinematics of fault bend folding: *Am. J. of Sci.*, v. 283, p. 648-721.
- Suppe, J., et al., 1997, Bed-by-bed fold growth by kink-band migration; Sant Llorenç de Morunys, eastern Pyrenees: Special issue; fault-related folding *Journal of Structural Geology*, v. 19, p. 443-461.
- Suppe, J.S., Chou, G.T., and Hook, S.C., 1992, Rates of folding and faulting determined from growth strata, *in* McClay, K.R., ed., *Thrust Tectonics*: London, Chapman and Hall, p. 105-122.
- Verges, J., et al., 1996, Unfolding; an inverse approach to fold kinematics: *Geology (Boulder)*, v. 24, p. 175-178.
- von Gosen, W., 1992, Structural evolution of the Argentine Precordillera; the Rio San Juan section: *Journal of Structural Geology*, v. 14, p. 643-667.
- Wells, D.L. and Coppersmith, K.J., 1994, New empirical relationships among magnitude, rupture length, rupture width, rupture area, and surface displacement: *Bulletin of the Seismological Society of America*, v. 84, p. 974-1002.
- Zapata, T.R. and Allmendinger, R.W., 1996, Thrust-front zone of the Precordillera, Argentina; a thick-skinned triangle zone: *AAPG Bulletin*, v. 80, p. 359-381.

## **Appendices**

## Structure Appendix

### Bedrock Geology

Three stratigraphic units were identified on the flanks of Sierra de Villicum through geologic mapping. These bedrock units include; undifferentiated Cambrian to Ordovician limestones and dolomites, Middle Neogene sandstones and conglomerates of the Las Tapias Formation, and upper Neogene conglomerates of the Mogna Formation. The Cambrian-to-Ordovician-age carbonate strata dominate the topographic relief of Sierra de Villicum and are the oldest rocks exposed in the Eastern Precordillera. Bedding orientations (dip/dip-dir) within carbonates along the western range front vary from steeply inclined (~70/119) and potentially overturned to ~56/252 near the southern tip of the range. Carbonate strata on the eastern side of the range have an orientation of ~50/145. An erosional contact (angular unconformity) between the Cambro-Ordovician carbonates and the middle Neogene-age Las Tapias Formation sandstones and conglomerates is identified by the presence of an angular carbonate block conglomerate with a red, fine-grained matrix. This contact was observed on both sides of Sierra de Villicum. Along the western contact, Las Tapias Formation strata have an orientation of ~69/128 that is roughly parallel to the carbonate bedding. Along the southern tip of the range front, Las Tapias Formation strata have an orientation of ~81/300 that decreases in dip away from the contact. On the western flank of Sierra de Villicum, the Las Tapias Formation sandstones and conglomerates have an

orientation of  $\sim 05/135$ . This shallowly dipping orientation extends  $\sim 5$  km SE of the contact. (This region corresponds with the Western Domain, region of relatively undeformed terrace surfaces, that is described in the main body of the thesis). Farther east, the Las Tapias Formation strata steepen to  $\sim 40/135$ . To the north, Las Tapias Formation strata increase to an orientation of  $\sim 64/116$  near the contact with the Mogna Formation conglomerates. In the southern portion of the study area, Las Tapias Formation strata transition to south dipping orientations ( $\sim 19/153$ ). The contact between the Las Tapias Formation and the Mogna Formation varies from north to south. In the southern portion of the study area, the contact is an angular unconformity where shallowly south dipping ( $\sim 07/183$ ) Mogna Formation conglomerates overlie interbedded sandstones and conglomerates of the Las Tapias Formation. The contact can be traced to the tip of Sierra de Villicum. The contact becomes  $\sim$  parallel to the strike of the Las Tapias Formation in the northern half of the study area. The Mogna has an orientation of  $\sim 21/110$  in a roadcut along the eastern margin of the study area. Age constraints on the Mogna and Las Tapias Formations are 4 Ma and  $\sim 8.5$  Ma respectively (Ramos and Vujovich, 2000). Based on the differing structural geometries between these two geologic units, deformation caused by and east-vergent basement-involved structure began prior to, or contemporaneously with deposition of the Mogna Fm. The unconformity between the Las Tapias and Mogna Formations is not present farther south (V. Ramos, pers comm.), suggesting that the fold growth was coeval with deposition of the Mogna.

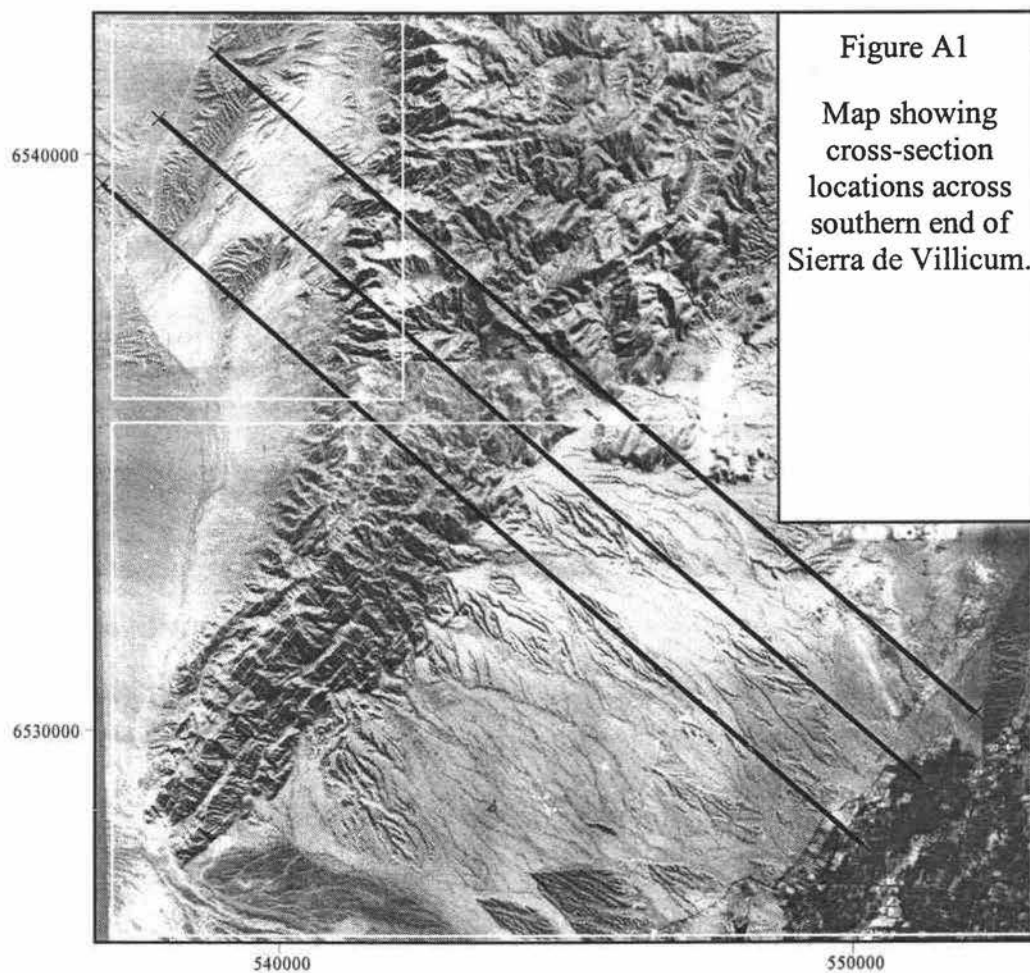
## **Geomorphology**

Five strath terraces were mapped on the eastern flank of Sierra de Villicum. The mapping and surveying of these terraces are described in the main body of the thesis. All of the short survey profiles (Figure 4) are presented in the Survey Appendix.

The spatial distribution of channels on the eastern side of Sierra de Villicum can provide additional information about the growth of the structure. Stream channels in the Western Domain are oriented ~ perpendicular to the trend of bedrock structure. Within the Eastern Domain, however, the orientations of stream channels vary N-S. In the south, the stream channels have a concave-S (deflected south) shape, while to the north, stream channels are ~ perpendicular to the structural trend.

## **Cross-sections**

Three geologic cross-sections were constructed across Sierra de Villicum to define the near-surface structure. The locations of the cross-sections are shown in Figure A1. Each NW-SE cross-section was constructed by projecting structural data, within 250m, onto the cross-section lines. The orientation of each cross-section ( $306^\circ$ ) is perpendicular to the overall trend of the structure. Figure A2 shows all three cross-sections.





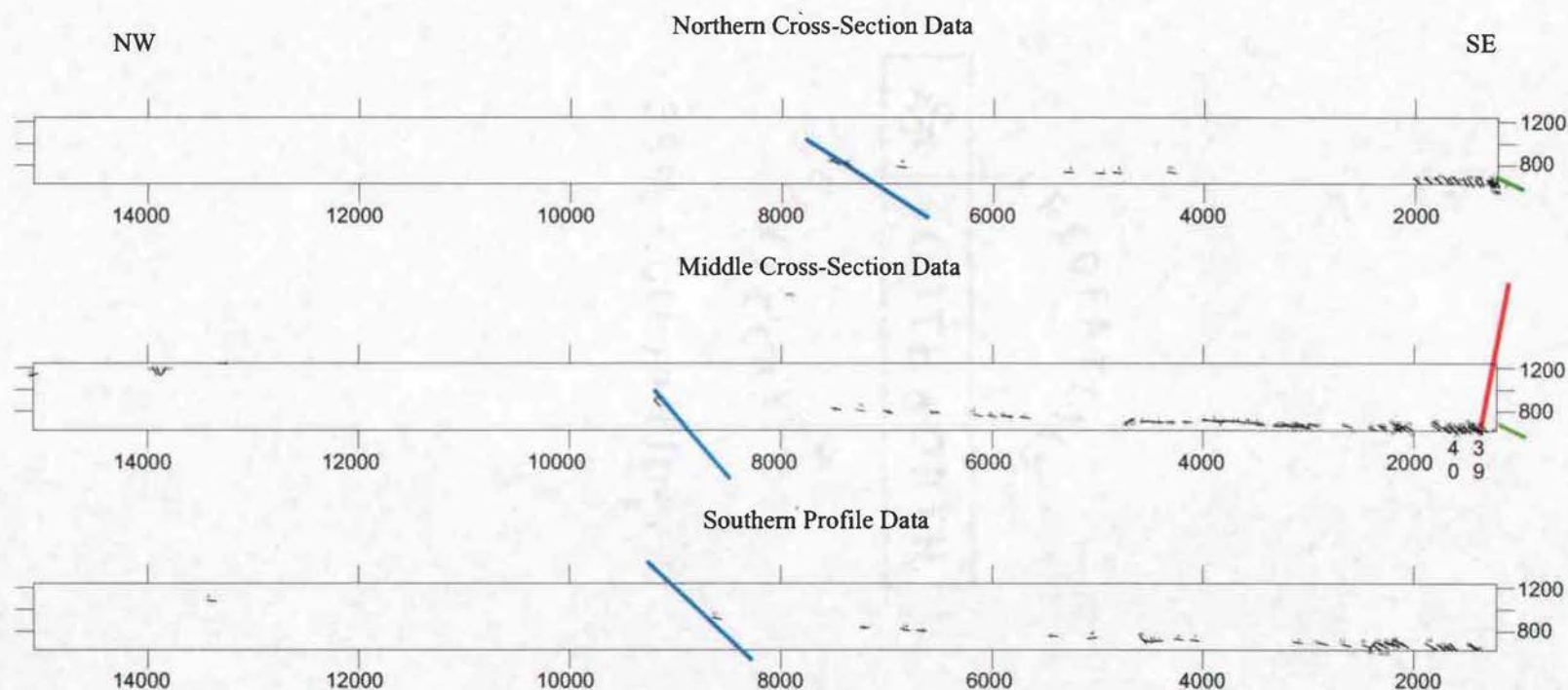


Figure A2 Cross-sections across the southern end of Sierra de Villicum. The location of profile lines is presented in Figure A1. A red line on the Middle Cross-Section shows the location of the interpreted active axial surface. Short black lines indicate the inclination of bedding along the cross-section. The blue lines represent the contact between the Cambro-Ordovician carbonates and the Las Tapias Formation sandstones. The green lines represent the contact between the Las Tapias and the Mogna Formation conglomerates. No vertical exaggeration.

### Crustal-Scale Model of Fold Growth

- The near surface structure of Sierra de Villicum resembles the geometry of a west-vergent fault-related-fold. The steep to overturned orientation of the carbonate strata on the western side of the range identifies the forelimb of the fold. This interpretation is also supported by the presence of successively steeper Neogene strata adjacent to the eastern range front. This fanning-upward geometry supports westward vergence of the structure. Because they are the oldest rocks exposed in the Eastern Precordillera, the decollement is most likely located within or at the base of the Cambrian to Ordovician age carbonates. To the west of Sierra de Villicum, von Gosen (1992) places the regional decollement of the Precordillera within Silurian strata, above the Cambro-Ordovician stratigraphic sequence. North of Sierra de Villicum, Zapata and Allmendinger (1996) show a west-vergent fault-related fold with a decollement at the base of the Neogene. Both studies interpret a very thin carbonate sequence associated with Sierra de Villicum.

- The overall geometry of the Neogene is what would be expected for growth strata formed on the backlimb of a fault-related-fold. The ~ flat geometry of the Las Tapias Formation strata on the backlimb of the structure and the lack of deformation within this zone suggest that it is located above a footwall ramp. The western boundary of this segment of the footwall ramp can be tentatively constrained by a change in Las Tapias bedding orientations from  $\sim 20^\circ$  to a dip of  $\sim 05^\circ$ . Along the northern cross-section, this proposed fold axis also corresponds with a change in the inclination of carbonate strata from  $\sim 50^\circ$  to  $\sim 35^\circ$ . The eastern

boundary of the footwall ramp segment can be constrained by the position of the fold axis separating  $\sim 05^{\circ}\text{E}$  and  $\sim 25^{\circ}\text{E}$  dipping Las Tapias sandstones and conglomerates. Because the Las Tapias strata were likely deposited contemporaneously with deformation of the carbonate strata, the position of the growth axial surface in older strata cannot be known without seismic profiles or well data.

- The folded terrace gravels reflect the migration of an active axial surface that folds  $\sim$  horizontal strata  $15^{\circ}$  clockwise (increased eastward inclination). This geometric relationship is also observed within the Neogene bedrock. West of the interpreted active axial surface, Neogene strata have an inclination of  $\sim 40^{\circ}$ , while to the east of the axial surface, Neogene sandstones have a dip of  $\sim 25^{\circ}$ . The folding of strath terraces requires that the underlying bedrock be folded by the same amount. This relationship suggests that the dip of the Las Tapias Formation sandstones, near the active axial surface, was  $\sim 25^{\circ}$  E prior to folding of the terrace surfaces. Therefore, an additional fault segment is needed to reconcile the geometry of the fault-related-fold. The fault segment has a dip of  $25^{\circ}\text{E}$  and extends to an eastern limit based on the trend of the s-plunging synclinal axis located in the basin  $\sim 3$  km to the north. At this location, the footwall ramp transitions to horizontal and is represented at the surface by a N-S trending syncline.

Bedrock geology, geomorphology, and crustal seismicity data (Smalley et al., 1993), were incorporated into a crustal-scale model of the growth of Sierra de Villicum Structure (Figures A3 & A4). This model shows that deformation related

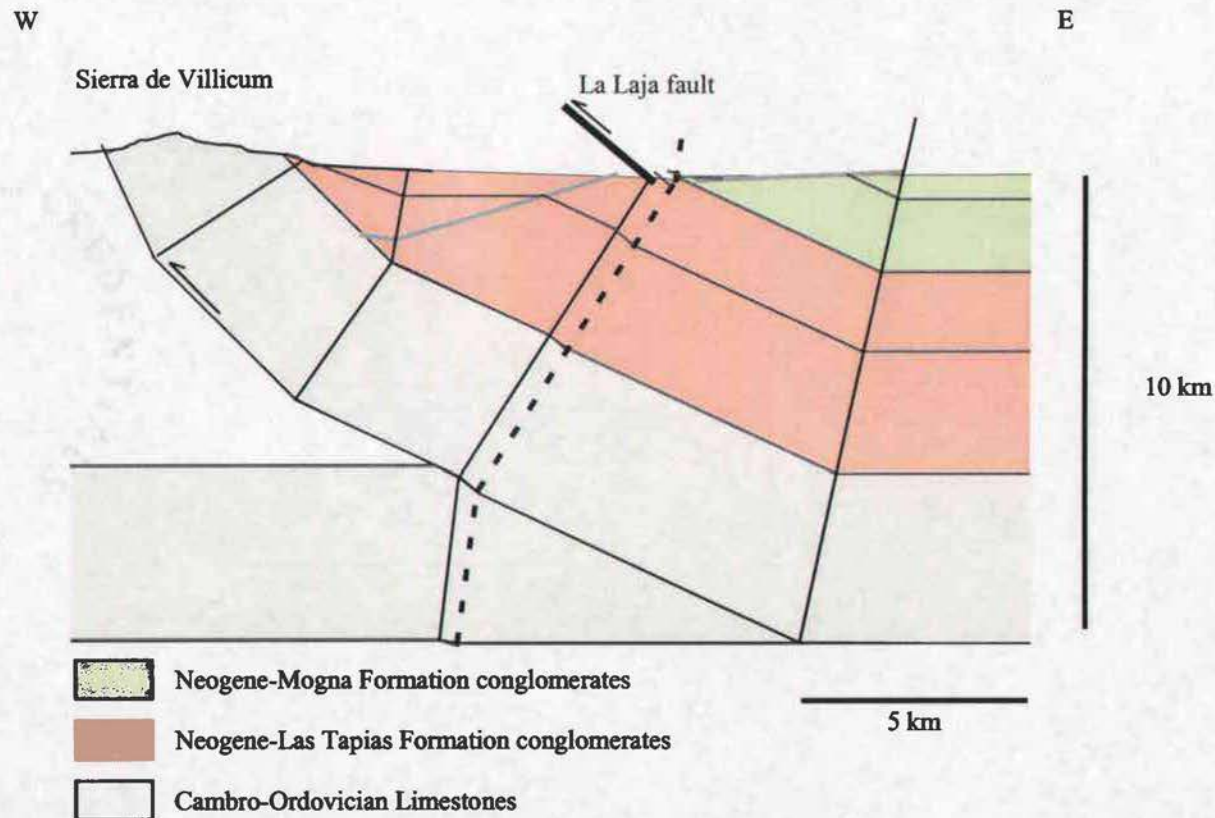


Figure A3 Enlarged crustal-scale model of fold growth for Sierra de Villicum, San Juan Argentina. The dashed line shows location of the interpreted active axial surface. The thick black line shows the location of the La Laja fault that experienced ~60cm of displacement in the Ms 7.4 earthquake in 1944. The thick gray lines represent the position of growth axial surfaces within the Neogene strata.



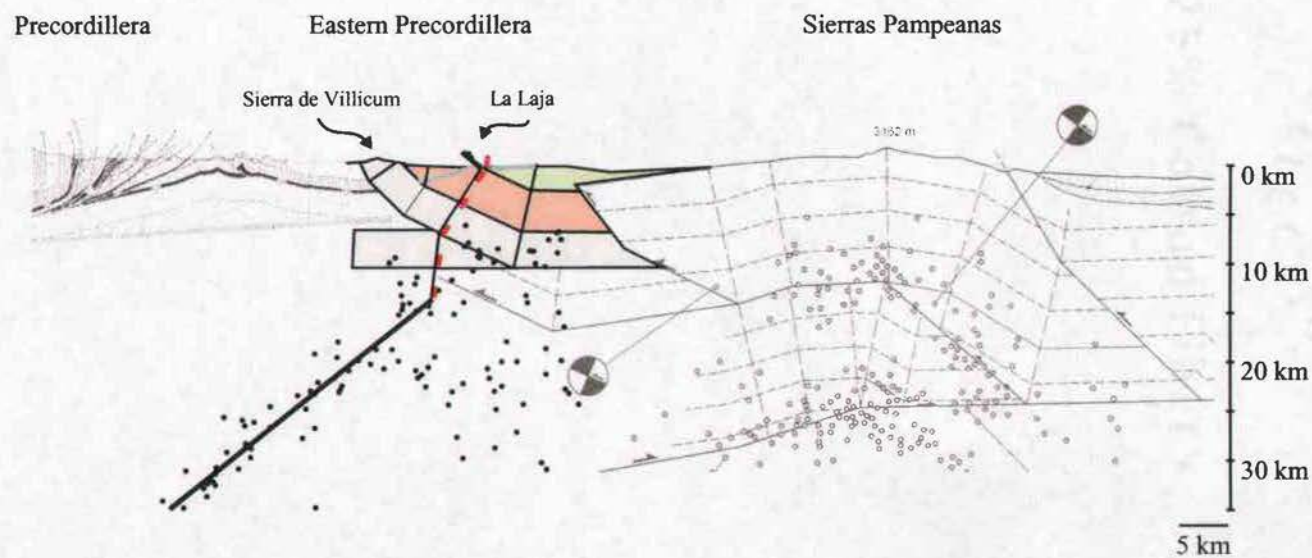


Figure A4 Crustal-scale model of fold growth for Sierra de Villicum, San Juan Argentina. The dashed red line represents the active axial surface. The thick gray lines represent growth axial surfaces. The black dots represent microseismicity data adapted from Smalley et al., 1993. Modified from von Gosen (1992) and Ramos et. al.,(2002). No vertical exaggeration.

to the 1944 earthquake reflects overprinting of a fault-bend-fold by an east-vergent, basement-involved structure at depth.

### **Moment Magnitude Calculations**

The equation  $M_w = 2/3 \log(M) - 6.0$  of Wells and Coppersmith (1994) where  $M = \text{fault area} * \text{fault slip} * \text{coefficient of elasticity}$  was used to evaluate the potential moment magnitude of faults that could have been the source of the 1944 Ms. 7.4 earthquake. Surface magnitude ( $M_s$ ) and moment magnitude ( $M_w$ ) are assumed to be equal for  $M_s < 7.5$  (Wells and Coppersmith, 1994). First examined was the La Laja fault. With a 6 km long surface rupture and 0.6 m of coseismic displacement, the only variable needed to calculate a magnitude is the down dip rupture length of the fault. Assuming that fault slip is directly related to fold growth, the down dip length would extend from the surface trace to the active axial surface (AAS). East of the AAS, the strata is unfolded and therefore would not support layer parallel slip. The resulting fault length of ~100 m yields a  $M_w$  of 4.8. If it is assumed that the La Laja fault represents slip tied to growth of the Sierra de Villicum fault-bend-fold (fbf), the length of the fault follows bedding dip from the surface to the synclinal axis of the fbf. Taking this measurement from the crustal-scale model (Figure A3), the La Laja fault has a down-dip length of 5.6 km and could produce a  $M_w$  6.0 earthquake. An alternative hypothesis is that the basal decollèment beneath the fault-bend-fold could have been the source of the earthquake. Measuring from the crustal-scale model (Figure A3) yields a down-dip fault length of ~ 20 km and a  $M_w$  of 6.3. Additionally, the 1944 fault could

have originated along the west-dipping zone of seismicity, between ~10 and 35 km depth, identified by Smalley et al., (1993). This basement fault has a down-dip length of ~ 34 km and a potential  $M_w$  of 6.5.

This exercise is important in ruling out the La Laja fault as the source fault for the 1944 earthquake. In order for the La Laja fault to create a  $M_w$  7.4 earthquake, it would need to be ~ 50000 km in length if it is caused by surface fold growth and ~ 1000 km if related to growth of the fbf. These lengths are several orders of magnitude larger than the 1944 surface rupture. This observation supports the interpretation of La Laja as a secondary flexural-slip fault. The rupture lengths associated with fbf growth and overprinting by a basement-involved structure are on the order of ~100 to 200 km. This is also larger than the observed surface rupture, however since the La Laja fault is interpreted as a secondary fault, the actual magnitude of fault slip is likely masked by distribution of slip on other faults and folds. Therefore, the scenarios of fbf or basement-involved fold growth are both possible explanations for the 1944 earthquake, however they cannot be distinguished from one another based on this information.

### **Discussion**

- Could the structure of Sierra de Villicum be explained as simply the growth of a fault-related-fold? The unusually high dips on the backlimb of the fold and eastward migration of an axial surface in a dominantly west-vergent structure preclude it from being entirely the result of fault-related-folding. FBF theory does not allow for dips steeper than ~ 30° on the backlimb of a structure. Additionally,

the steeply dipping segments would require that the active axial surface is currently folding pregrowth strata, requiring a large amount of slip on the decollement.

Another argument for overprinting comes from the seismicity data. The seismicity data describe a west-dipping plane of focused seismicity that extends to a depth of ~35km and therefore involves an east-vergent basement structure at depth. The upper boundary of the seismicity seems to roughly correspond with the proposed depth of the decollement determined from structural reconstruction. Additionally, the position of the basement fault/fault-related-fold intersection roughly correlates with the position of the active axial surface. Each of the datasets supports a model where Sierra de Villicum is a west-vergent fault-related-fold that is being overprinted by an east-vergent basement involved structure at depth.

- The crustal scale model is in agreement with similar models and structures described by von Gosen(1992), Zapata and Allmendinger (1996), and Ramos et al., (2002) (Figure A4). To the west, the Precordillera shows eastward thinning of the Paleozoic sequence with a decollement located at the base of the Devonian strata. The overall structure of Sierra de Villicum shows a west-vergent fault bend fold geometry with a decollement level within or at the base of the Cambro-Ordovician carbonates. To the west, the Precordillera thrust sheets have a decollement at the top of the Cambro-Ordovician strata (von Gosen, 1992). This interpretation supports the observation of older rocks exposed within the Eastern Precordillera. To the east, seismicity data beneath Pie de Palo (one of the Sierras Pampeanas basement-involved uplifts) can be used to interpret an east-dipping



range bounding fault. A Sierras Pampeanas uplift (valle Fertil), to the north of the study area, was interpreted to have a similar geometry (Zapata and Allmendinger, 1996).

### **Conclusion**

Recent deformation (1944) on the eastern flank of Sierra de Villicum reflects overprinting of a west-vergent fault-bend-fold by displacement along an underlying east-vergent basement thrust.

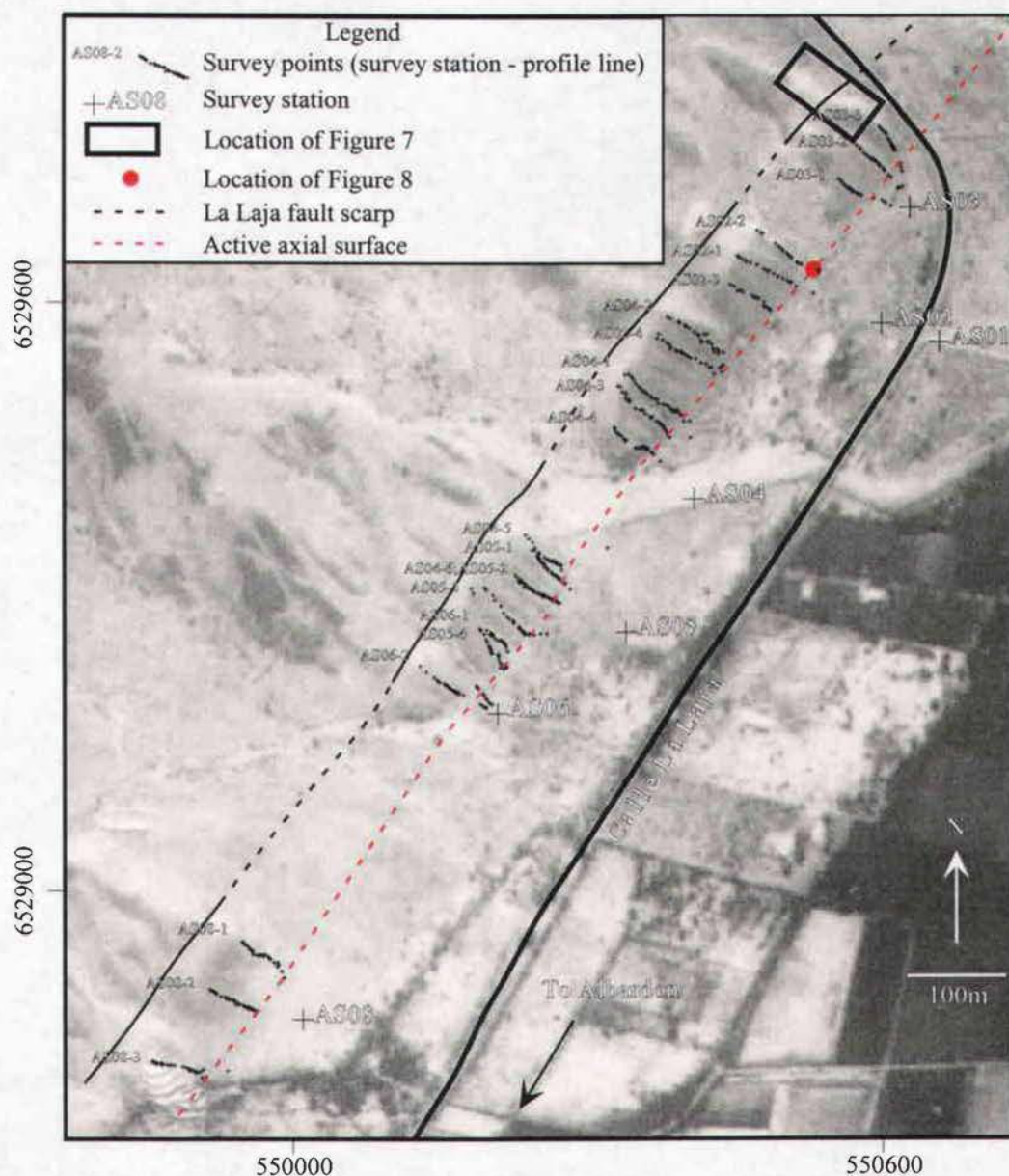


Figure B1 Map showing the location of survey profiles. Each of the profiles were created with the use of a laser ranging theodolite and handheld GPS receiver. The large plus symbols represent survey stations and the smaller text AS0#-# represent individual survey lines. All of the survey data for each profile was plotted on a common profile line trending 306 degrees. This profile was the angle where all of the survey data was clustered together. This angle is also close to the structural trend of Sierra de Villicum.

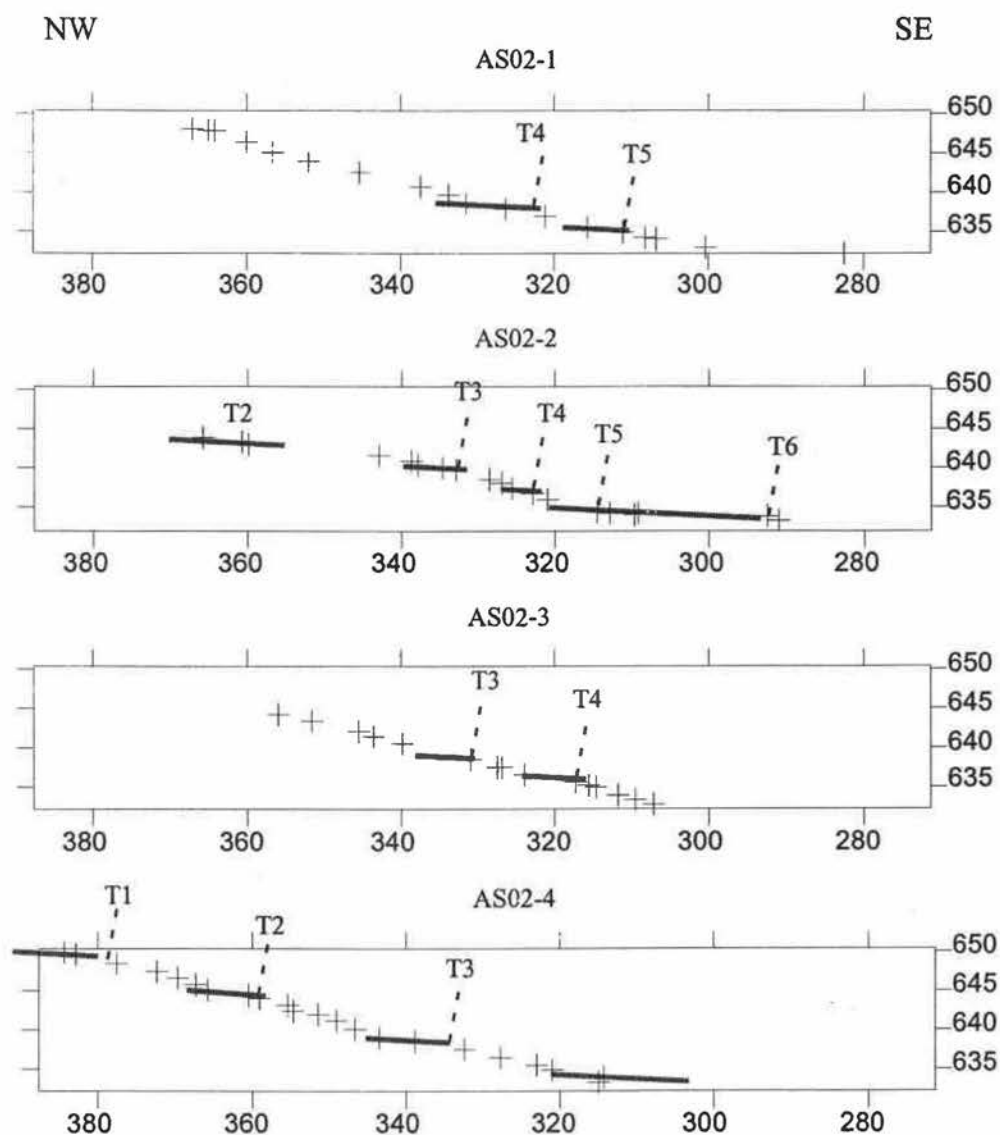


Figure B2 AS02 Topographic Profiles. Survey data points are represented by a plus symbol. The gray lines represent the position of a terrace tread. Thin dashed lines mark the position of a growth axial surface. AS02-# refers to the survey station and profile number. The positions of survey stations and profiles are shown on Figure B1.

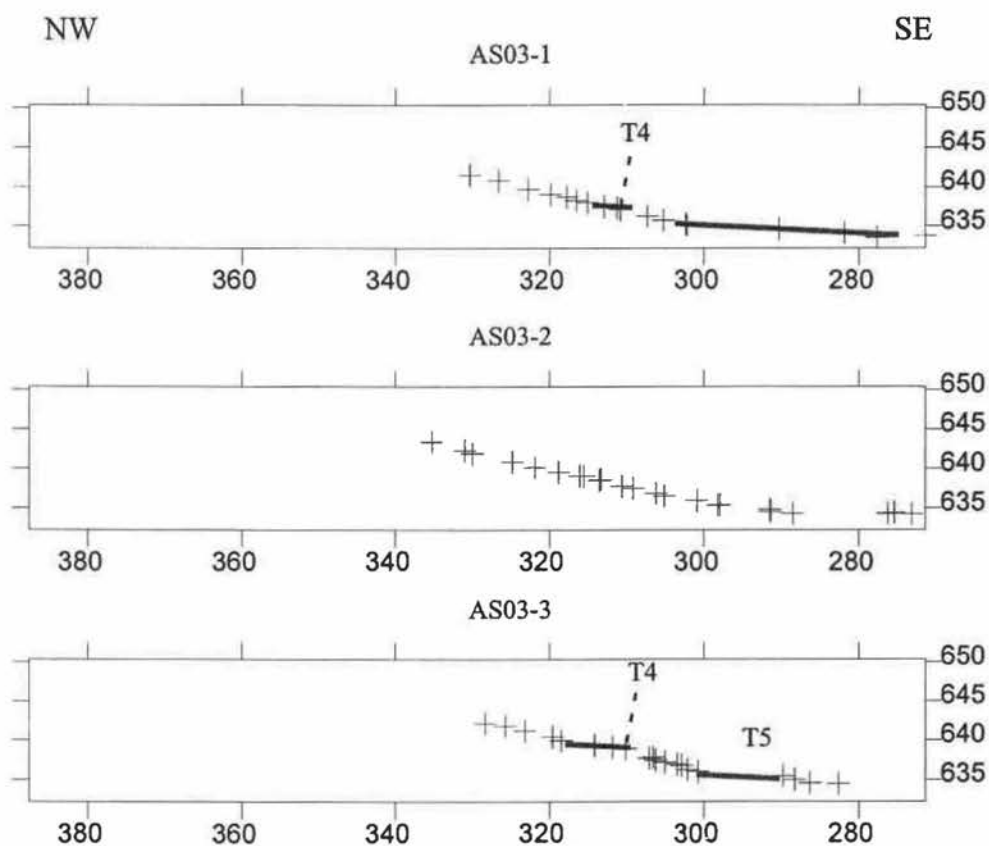


Figure B3 AS03 Topographic Profiles. Survey data points are represented by a plus symbol. The gray lines represent the position of a terrace tread. Thin dashed lines mark the position of a growth axial surface. AS03-# refers to the survey station and profile number. The positions of survey stations and profiles are shown on Figure B1.

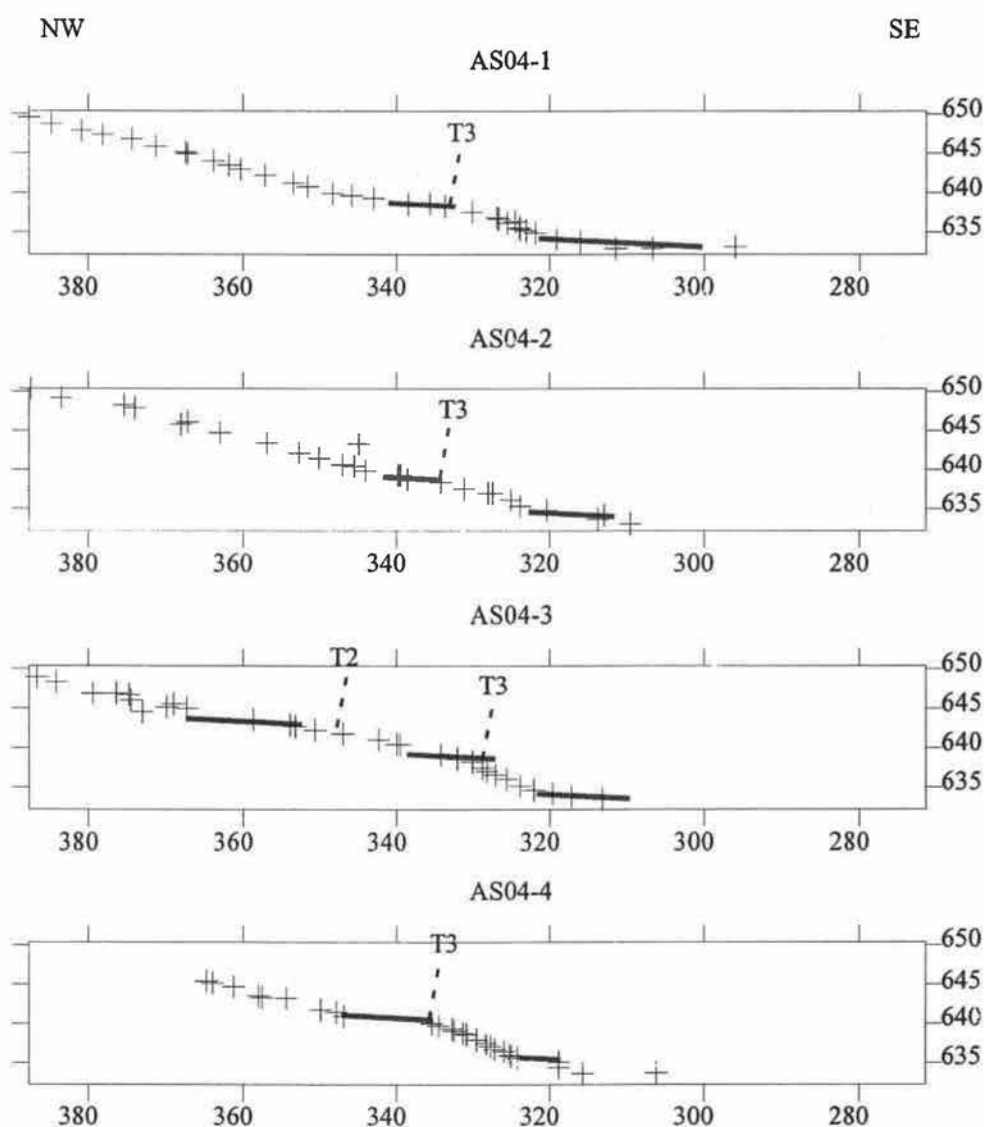


Figure B4 AS04 Topographic Profiles. Survey data points are represented by a plus symbol. The gray lines represent the position of a terrace tread. Thin dashed lines mark the position of a growth axial surface. AS04-# refers to the survey station and profile number. The positions of survey stations and profiles are shown on Figure B1.

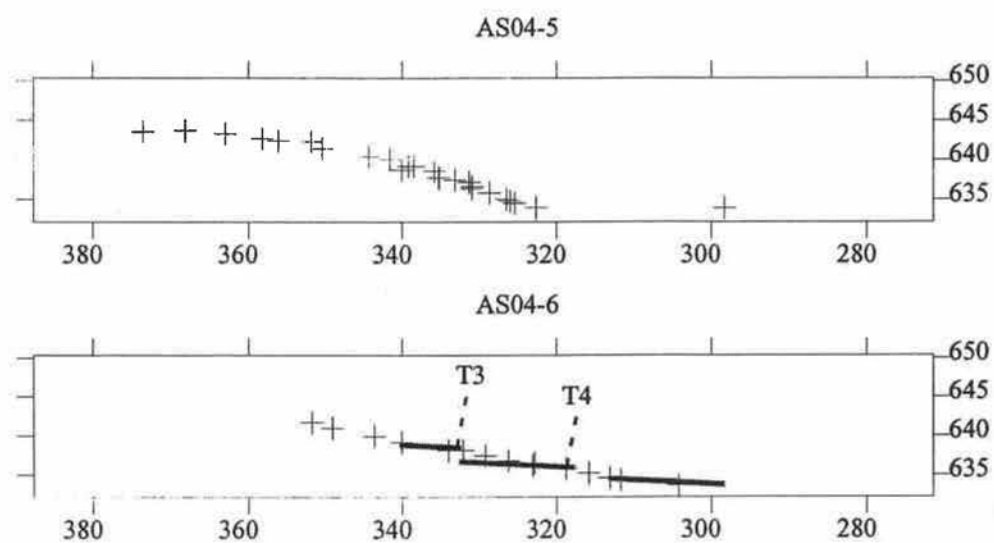
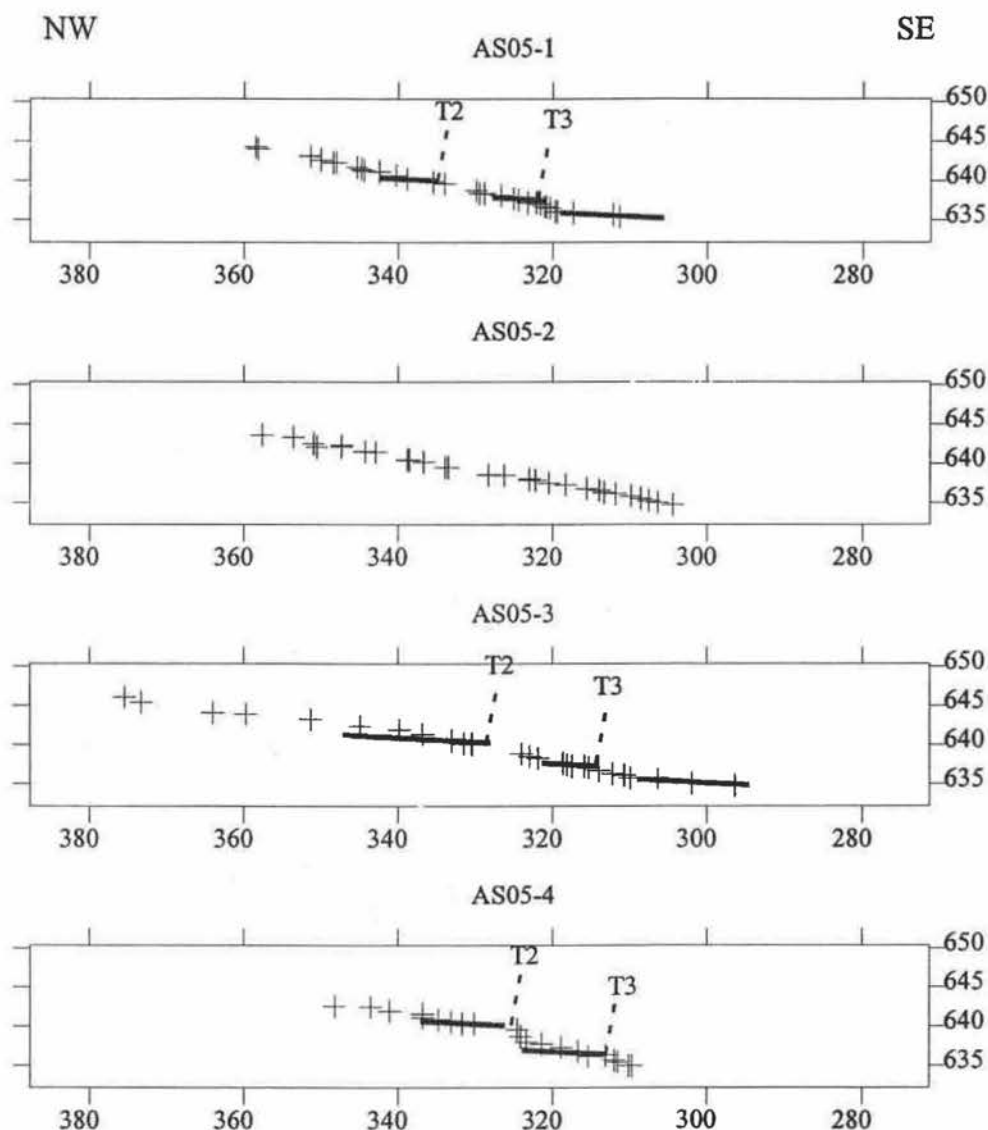


Figure B4 (continued).





**Figure B5** AS05 Topographic Profiles. Survey data points are represented by a plus symbol. The gray lines represent the position of a terrace tread. Thin dashed lines mark the position of a growth axial surface. AS05-# refers to the survey station and profile number. The positions of survey stations and profiles are shown on Figure B1.

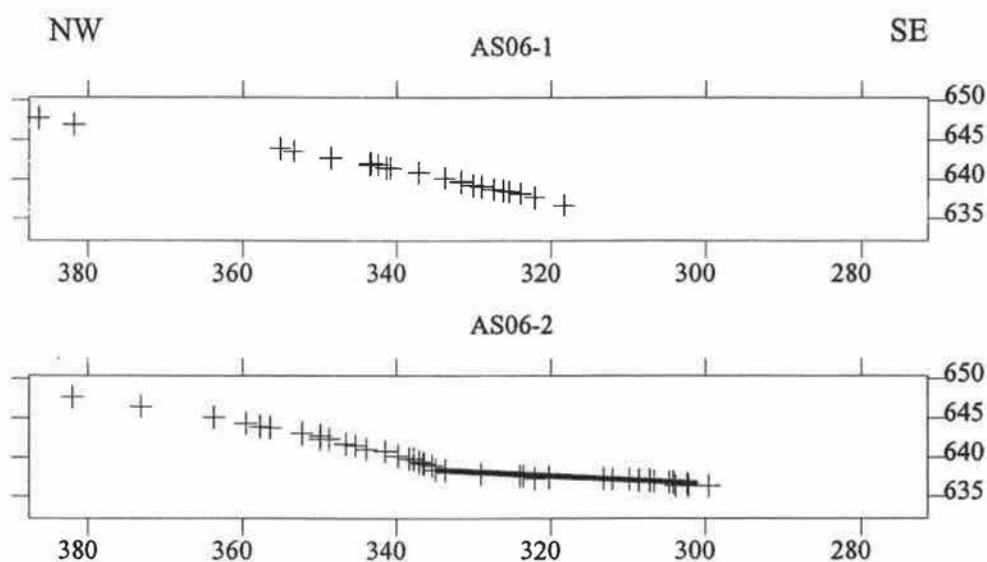


Figure B6 AS06 Topographic Profiles. Survey data points are represented by a plus symbol. The gray lines represent the position of a terrace tread. Thin dashed lines mark the position of a growth axial surface. AS06-# refers to the survey station and profile number. The positions of survey stations and profiles are shown on Figure B1.

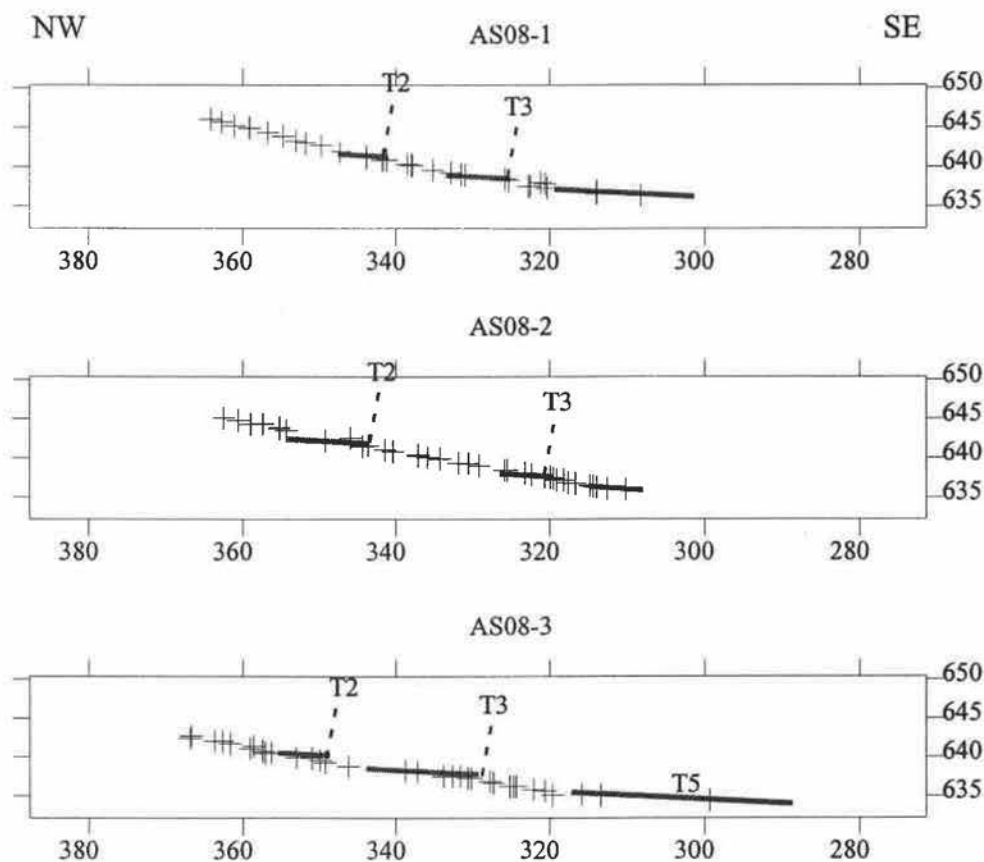


Figure B7 AS08 Topographic Profiles. Survey data points are represented by a plus symbol. The gray lines represent the position of a terrace tread. Thin dashed lines mark the position of a growth axial surface. AS08-# refers to the survey station and profile number. The positions of survey stations and profiles are shown on Figure B1.